A E R O N O M Y R E P O R T

N O. 14

COLLISION FREQUENCIES AND ELECTRON TEMPERATURES IN THE LOWER IONOSPHERE

by

J. E. Salah

S. A. Bowhill

August 15, 1966

Supported by
National Aeronautics and Space Administration
Grant NsG-511

Aeronomy Laboratory
Department of Electrical Engineering
University of Illinois
Urbana, Illinois

ACKNOWLEDGEMENT

Principal thanks go to the author's thesis advisor, Professor S. A. Bowhill, for his guidance throughout the course of this research work. Thanks are also due to the Aeronomy Laboratory staff for carrying out the computations and typing the manuscript.

The work described in this report was supported by the National Aeronautics and Space Administration under grant NsG-511.

ABSTRACT

The question of thermal equilibrium in the lower ionosphere has recently led to several conflicting theories. In this report, a method for the extraction of electron and neutral temperatures from experimental data is described, and the results of application to several rocket flights are presented. The electron temperature is derived from the electron collision frequency which is determined by propagation techniques. This involves the measurement of the differential absorption and Faraday rotation of two waves propagating in the ionosphere. The neutral temperature is obtained from the scale height of molecular oxygen, determined from the measurement of the absorption of solar ultraviolet radiation. The various experimental and analytical techniques are described in detail.

TABLE OF CONTENTS

TABLE OF CONTENTS (continued)

LIST OF ILLUSTRATIONS

LIST OF ILLUSTRATIONS (continued)

LIST OF TABLES

1. Introduction

One of the primary properties of the atmosphere is its temperature. It is used to describe the structure of the atmosphere, and leads to a classification of the various height regions such as the troposphere, stratosphere, mesosphere, and thermosphere. In the ionosphere, where free electrons exist in significant number, it is important to consider the electron temperature and to compare it with the temperature of the neutral gas. These temperatures govern various energy distributions, kinetic parameters, such as recombination coefficients, flux rates of chemical reactions, and are essential components of almost every formulation pertaining to the ionosphere.

The comparison of electron and neutral temperatures leads to the important question of thermal equilibrium in the ionosphere. Thermal equilibrium means that there is an equal energy transfer between the electrons and the neutral gas, which implies equality of temperatures. This has been recently examined by several investigators. Above 150 km, evidence has been accumulated in favor of electron temperature exceeding the neutral temperature (Evans and Lowenthal, 1964; Brace et al., 1965). Between 90 and 150 km, Langmuir probe measurements have shown that the electron and neutral temperatures are unequal, but this result remains under debate.

Below 90 km, this problem has lead to several conflicting theories. From a study of photodetachment of electrons from ions, Sears (1965) concludes that the electron temperature may exceed the neutral temperature, and supports cross-modulation observations made by Rumi (1962), which

revealed a high electron temperature. Belrose and Hewitt (1964) also support the non-equilibrium hypothesis, based on the collision frequency correlation with solar activity. On the other hand, Dalgarno and Henry (1965) have studied in detail the rates of energy loss of electrons in the D-region and have concluded that thermal equilibrium exists at these altitudes.

There has been so far no way of measuring directly the electron temperature below 100 km, where Langmuir probe theory becomes invalid. It is the purpose of this work to describe a method of extracting the electron temperature from the collision frequency of electrons with neutrals. It is based on the laboratory measurements of Phelps and Pack (1959) which revealed that the electron collision frequency in air is directly proportional to the electron energy. The collision frequency is obtained from radio propagation experiments, which measure the Faraday rotation and differential absorption of a radio wave propagated from the ground and through the lower regions of the ionosphere. The neutral temperature is obtained independently from the scale height of molecular oxygen, determined from the absorption of the sun's ultraviolet radiation. A comparison of electron and neutral temperatures is then possible.

In outline, Chapter 2 reviews several relevant aspects of the propagation theory, namely, the Appleton-Hartree formulas and the quasi-longitudinal approximation, and the generalized Appleton-Hartree theory, as applied to the analysis. Chapter 3 deals with the experimental techniques, description of the payloads and the ground station, and the

reduction of the data. Development of the formulas to obtain electron densities and extract collision frequencies from the radio propagation data is described in Chapter 4. Chapter 5 is concerned with the determination of molecular oxygen concentration and atmospheric pressure from the ultraviolet absorption measurements. In brief, Chapters 2 to 5 describe the methods which provide the necessary parameters in the calculation of electron and neutral temperatures. In Chapter 6, the theories pertaining to thermal equilibrium conditions are described in detail, and a formulation of electron temperature in terms of collision frequency is developed. The analysis is then applied to five rocket experiments launched under varying conditions, and the results are presented.

2. RELEVANT ASPECTS OF PROPAGATION THEORY IN THE IONOSPHERE

Prior to the description of the radio propagation experiment and the presentation of its results, it is necessary to understand the properties of the ionosphere, as expressed by the formulas of the magneto-ionic theory. For this purpose, the Appleton-Hartree formula is rederived in this chapter with the omission of algebraic details; and the quasi-longitudinal approximation is discussed with respect to its application to this analysis. The third section deals with the generalized magneto-ionic formulas and their importance in this study.

2.1 The Classical Appleton-Hartree Theory

It is well known that in the presence of an imposed magnetic field, a wave traveling in an ionized medium is split into the two characteristic components of the magneto-ionic theory. The ionization in the ionosphere together with the earth's magnetic field, lead to similar splitting of a propagating wave. The resultant waves are elliptically polarized, with opposing senses of rotation, and lead to two complex indices of refraction (Ratcliffe, 1959).

The formulas for the index of refraction in the ionosphere, commonly called the Appleton-Hartree formulas (Appleton, 1932; Hartree, 1931), have been derived with the assumption that the electronic collisions are independent of the electron energy. The assumed properties of the medium include electric neutrality, uniform charge distribution, uniform external magnetic field, and stationary ions.

For a wave of angular frequency ω, propagating in the positive z-direction (defined upwards), the electric vector is given by

$$\underline{E} = E_o \exp\ j(\omega t - kz) \ , \tag{2.1}$$

where E_o is the field at some reference altitude, and may be complex. The wave propagation constant, k, is connected to the wavelength λ by

$$k = \frac{2\pi}{\lambda} \ . \tag{2.2}$$

Two components of the electric vector are present, one in the x-direction, E_x, and the other in the y-direction, E_y. These are related by the polarization R of the wave, which is defined by

$$R = \frac{E_x}{E_y} \ . \tag{2.3}$$

Inserting a field variation of the form expressed by Equation (2.1) in Maxwell's equations for any homogeneous medium, one obtains an expression for the complex refractive index, n, given by

$$n^2 = 1 + \frac{P_x}{\varepsilon_o E_x} = 1 + \frac{P_y}{\varepsilon_o E_y} \ , \tag{2.4}$$

where n is defined by

$$n = \frac{k}{\omega\sqrt{\varepsilon_o \mu_o}} \ , \tag{2.5}$$

and where ε_o and μ_o are the capacitivity and permeability of free space, respectively; and P_x and P_y are the polarization fields in the x and y directions.

Furthermore, when an electromagnetic wave is incident on a plasma in the presence of a magnetic field and collisions, it is best to consider the motion of an individual electron. Despite the electric neutrality condition of the plasma, the effect of positive ions can be neglected because of the great difference in mass between the electron and the ion. When the electron of mass m, and charge e, is subjected to an electric field $\underline{E}$, it is governed by the equation of motion

$$m\ddot{\underline{r}} + m\nu\,\dot{\underline{r}} = -e(\dot{\underline{r}} \times \underline{B}) - e\underline{E} \ , \tag{2.6}$$

where ν is the electron-neutral collision frequency and $\underline{B}$ is the flux density of the magnetic field. The displacement of the electron from its rest position, $\underline{r}$, is related to the dielectric polarization $\underline{P}$ by the equation

$$\underline{P} = - N e \underline{r} \ , \tag{2.7}$$

where N is the electron density.

The following accepted symbols are then introduced:

$$Z = \frac{\nu}{\omega} \quad , \tag{2.8}$$

$$X = \frac{\omega_N^2}{\omega^2} = \frac{Ne^2}{\varepsilon_o m\omega^2} \quad , \tag{2.9}$$

$$Y = \frac{\omega_H}{\omega} = \frac{eB}{m\omega} \quad , \tag{2.10}$$

where the ω_N is plasma frequency and ω_H is the gyrofrequency.

Two components of Y in the (x,z) plane are chosen, one in the longitudinal direction of the wave, Y_L, and the other in the transverse direction, Y_T. Equations (2.6) and (2.7) may then be expressed in a tensor relationship

$$\varepsilon_o \underline{E} = \underline{M}^{-1} \underline{P} \quad , \tag{2.11}$$

where M is a tensor susceptibility expressed by the inverted matrix

$$M^{-1} = -X^{-1} \begin{pmatrix} 1-jZ & jY_L & -jY_T \\ -jY_L & 1-jZ & 0 \\ jY_T & 0 & 1-jZ \end{pmatrix} \tag{2.12}$$

Manipulation of the above constitutive relations and combination with Maxwell's equations yield the following equation for the wave polarization

$$R^2 + j \frac{Y_T^2 / Y_L}{1-X-jZ} R + 1 = 0 \quad . \tag{2.13}$$

The roots of Equation (2.13) provide the two propagation modes whose polarizations, R_1 and R_2, represent two waves of circular polarization $\pm j$, rotating in opposite senses. The solution of the quadratic Equation (2.13) yields

$$R = -j\left\{\frac{Y_T^2/2Y_L}{1-X-jZ} \mp \sqrt{1+\frac{Y_T^4/4Y_L^2}{1-X-jZ}}\right\}. \qquad (2.14)$$

By substituting Equation (2.14) in Equation (2.4) we obtain an expression for the complex refractive index

$$n^2 = 1 - \frac{X}{1-jZ-jY_L R}. \qquad (2.15)$$

Equation (2.15) is called the Appleton-Hartree formula. The behavior and properties of the refractive index can be simplified in special cases when either the magnetic field or collisions are neglected, but these cases will not be discussed here. However, the important property of reflection of the magneto-ionic waves by the ionosphere will now be considered. Snell's law states that for a wave incident at an angle i to the normal, the angle ϕ with the normal at a level where the refractive index is μ is given by

$$\mu \sin\phi = \mu_o \sin i. \qquad (2.16)$$

But $\mu_o = 1$ outside the ionosphere, and at reflection $\phi = 90^o$, so that the refractive index at reflection, μ_r, must be equal to sin i. With normal

incidence (i=0) the condition of reflection becomes $\mu_r = 0$. Thus if the electron density is sufficiently large to reduce μ to zero at some altitude, then a normally incident wave will be reflected. Otherwise the wave will penetrate through the layer. Neglecting collisions, an expression for μ^2 may be derived from Equations (2.14) and (2.15). Setting $\mu = 0$ and solving for X it is found that one component, called the "ordinary" wave is reflected at X = 1, as in the absence of magnetic field. The other component, called the "extraordinary" wave, is reflected at either X = 1 + Y or X = 1 - Y depending on whether the propagation frequency is smaller or larger than the gyrofrequency.

2.2 The Quasi-Longitudinal Approximation

There are two limiting cases associated with the index of refraction, one of which applies when waves are propagated parallel to the direction of the magnetic field, the other perpendicular to it. When these cases are applied to the refractive index formula, the solutions are called longitudinal and transverse. Furthermore, when the condition expressed in Equation (2.17) is satisfied, the solution is called quasi-longitudinal. In this analysis we are concerned with radio waves propagating upwards through the ionosphere at mid-latitudes in the Northern hemisphere, and the quasi-longitudinal approximation is both adequate and valid.

The necessary condition to be satisfied in this case is

$$\left| Y_T^2 / 2Y_L \right| << \left| 1 - X - jZ \right|, \qquad (2.17)$$

which reduces the polarization expressed by Equation (2.14) to

$$R = \pm j . \tag{2.18}$$

The +j and -j refer to circularly polarized extraordinary and ordinary modes respectively. The condition in Equation (2.17) is fulfilled in this case because the angle between the magnetic field direction and the z-axis is very small and Y_T is therefore smaller than Y_L. From Equation (2.15), the corresponding form for the refractive index is then given by

$$n^2 = 1 - \frac{X}{1-jZ\pm Y_L} , \tag{2.19}$$

where now, the plus sign in front of Y_L refers to the ordinary wave and the minus sign to the extraordinary wave.

In the D- and lower E-regions of the ionosphere, where the electron density seldom exceeds 10^4 cm^{-3}, a further approximation of Equation (2.19) is appropriate. For electron densities of this order, the plasma frequency, f_N, defined by

$$f_N = \frac{1}{2\pi}\left(\frac{Ne^2}{\varepsilon_o m}\right)^{\frac{1}{2}} \tag{2.20}$$

is always much smaller than the propagation frequency (2 mc). Therefore $X \ll 1$, and the index of refraction expressed in Equation (2.19) may be approximated by

$$n \simeq 1 - \frac{\frac{1}{2} X}{1-jZ\pm Y_L} . \tag{2.21}$$

Further algebraic manipulations yield an expression for n in terms of real and imaginary parts given by

$$n = 1 - \frac{1}{2}\frac{X(1\pm Y_L)}{(1\pm Y_L)^2+Z^2} - j\,\frac{1}{2}\,\frac{XZ}{(1\pm Y_L)^2+Z^2} \,. \tag{2.22}$$

The complex refractive index expressed above may be expressed by definition as

$$n = \mu - j\chi \,, \tag{2.23}$$

where

$$\mu = 1 - \frac{\frac{1}{2}X(1 \pm Y_L)}{(1 + Y_L)^2 + Z^2} \,, \tag{2.24}$$

and

$$\chi = \frac{1}{2}\frac{XZ}{(1 \pm Y_L)^2 + Z^2} \,. \tag{2.25}$$

The meaning of these two parameters, μ and χ, is found from the form of the traveling wave expressed in Equation (2.1) with

$$k = k_o\, n \,, \tag{2.26}$$

where k_o is the phase constant in free space defined by

$$k_o = \frac{2\pi}{\lambda_o} = \frac{2\pi f}{c} \,, \tag{2.27}$$

and where c is the speed of light.

The resulting field may then be written as

$$E = E_o \exp(-\chi_o k_o z) \exp j(\omega t - \mu k_o z) . \quad (2.28)$$

Equation (2.28) represents a phase shifted wave whose amplitude is decreasing exponentially with distance. The phase in radians is given by $\mu k_o z$, and therefore, μ is called the phase refractive index. The decay in amplitude per unit distance is measured by the absorption coefficient κ defined as

$$\kappa = k_o \chi \quad (2.29)$$

The relative change in the phase refractive index of the two characteristic propagation waves is a measure of the angle of rotation of the electric field vector after passage through an ionization slab. This effect, usually called Faraday rotation, is useful for measuring electron densities, since by Equation (2.24), μ is directly related to N. Similarly, the measurement of absorption of a traveling radio wave may be used in conjunction with the electron density measured by Faraday rotation to obtain the electron collision frequency, since by Equation (2.25), χ is related to both N and ν. These relations will be developed in detail in a following chapter.

2.3 The Generalized Appleton-Hartree Theory

In the derivation of the Appleton-Hartree formulas it was assumed that the collision frequency was independent of the electron velocity. The energy dependence of the collision frequency was established by

Phelps and Pack (1959), whose laboratory results showed that ν is directly proportional to the electron energy. This same result will be used later for the computation of electron temperatures from collision frequency measurements.

Based upon the Phelps and Pack result, Sen and Wyller (1960) rederived the expressions for the complex refractive index and the state of polarization of a slightly ionized gas, in the presence of an external magnetic field and an oscillating electric field. The effects of the velocity dependence of the collision frequency were evaluated in closed analytic forms. In the general case where $\nu = \nu_m f(v)$, a new angular dependent term appeared, the coefficient of which vanished, when ν was assumed constant. The refractive index, then, was the same as that given by the Appleton-Hartree formula.

By taking into account the velocity dependence of the collision frequency, a proper averaging of the conductivity tensor elements was accomplished. The generalized conductivity tensor thus obtained was found valid for any velocity distribution function. Since in ionospheric wave propagation, the electrons are assumed to have a Maxwellian velocity distribution, the elements of the tensor were found to be expressible in terms of previously tabulated integrals. These integrals are called "C script" integrals and have been tabulated by Dingle, et al., (1957), and by Burke and Hara (1963).

The general expression is given by

$$\mathcal{G}_p(x) = \frac{1}{p!} \int_0^\infty \frac{\varepsilon^p e^{-\varepsilon}}{\varepsilon^2 + x^2} \, d\varepsilon \quad , \tag{2.30}$$

where

$$\varepsilon = \frac{mv^2}{2kT} \quad , \tag{2.31}$$

v is the electron velocity, m is the electronic mass, k is Boltzman's constant, and T is the temperature.

With the substitution of the symbols defined in Equations (2.8), (2.9), and (2.10), the expressions derived by Sen and Wyller for the complex refractive index may be written as

$$n^2 = (\mu - j\chi)^2 = 1 - \frac{X(1 \pm Y_L)}{Z_m^2} \mathcal{G}_{3/2}\left\{\frac{1 \pm Y_L}{Z_m}\right\} - j\frac{5}{2}\frac{X}{Z_m} \mathcal{G}_{5/2}\left\{\frac{1 \pm Y_L}{Z_m}\right\} \quad , \tag{2.32}$$

where

$$Z_m = \frac{\nu_m}{\omega} \quad . \tag{2.33}$$

The parameter ν_m used in the generalized theory represents the mean collision frequency associated with the square of the most probable speed. The subscript m stands for monoenergetic, which refers to electrons of energy kT.

When the energy dependence of the collision frequency was taken into

account, it was found that the absorption factors based on the generalized theory differed from those based on the classical Appleton-Hartree theory by amounts varying from 30 to 100 percent. It was then found that improved agreement is obtained when the collision frequency in the Appleton-Hartree formula, henceforth called ν_{AH} is associated with the mean energy, namely

$$\nu_{AH} = \frac{3}{2}\nu_m \cdot \tag{2.34}$$

Assuming that the electron gyrofrequency is of the same order as the propagation frequency, correction factors have been calculated and may be applied to the Appleton-Hartree collision frequencies. In the asymptotic limit $\nu << \omega(1 \pm Y_L)$, the Appleton-Hartree formula can be retained provided that ν_{AH} is replaced by

$$\nu_{AH} = \frac{5}{2}\nu_m \cdot \tag{2.35}$$

In the other asymptotic limit $\nu >> \omega(1 \pm Y_L)$,

$$\nu_{AH} = \frac{3}{2}\nu_m \cdot \tag{2.36}$$

In the intermediate case, however, large errors in the absorption factor persist and no exact correction factor can be applied. The Appleton-Hartree theory, then, cannot be retained for this case and the generalized theory has to be applied.

The application of this theory to the present analysis was found to be quite important at the lower altitudes, where the approximation $Z < 1$ failed to hold. In general, although the analysis has been conducted using the Appleton-Hartree formula, some of the results, such as collision frequency, have been corrected by the multiplicative factors of the generalized theory.

3. OUTLINE OF THE EXPERIMENT

During the International Quiet Sun Years (1964-1965), series of Nike-Apache rockets, carrying specially instrumented payloads to study the lower regions of the ionosphere, have been launched from Wallops Island, Virginia. The aim of the experimental program has been to investigate the behavior of the D- and E-regions of the ionosphere under varying diurnal, seasonal and latitudinal conditions. The ionospheric parameters obtained and studied have been electron density, by measurement of Faraday rotation, standing wave and electron current; collision frequency, by differential absorption; molecular oxygen density, by ultraviolet absorption; electron temperature and positive ion density, by Langmuir probe. The experiments have been conducted by the University of Illinois in cooperation with the GCA Corporation, Bedford, Massachusetts.

In this chapter, the principle of the radio propagation experiment, the instrumentation of the payload and the ground station, and the data reduction techniques, are described in detail. Other payload experiments are described briefly.

3.1 Principle of Faraday Rotation and Differential Absorption Measurements Using Ground-based Transmitters and Rocket-borne Receivers

As explained in Section 2.2, the principle of the radio measurement of electron density is a comparison of the difference in attenuation coefficients and phase velocities of the ordinary and extraordinary magneto-ionic components. Since both parts of the refractive index are functions of frequency, it is important to choose a frequency low enough

to yield significant differential absorption and yet have enough signal left to measure the Faraday rotation. The range of 2 to 4 mc has been chosen for this experiment to satisfy various ionospheric conditions. At these frequencies and at medium latitudes, Wallops Island (40^{o}N), the polarizations are nearly circular and the extraordinary component is much more heavily absorbed than the ordinary, in the D-region. Therefore, through a modification of the Seddon (1958) technique, two oppositely, circularly polarized waves, differing in frequency by 500 cps, are transmitted from the ground. A polarization ellipse is thus generated, spinning at a rate of 250 rps, as shown in Figure 3.1. This resultant elliptical polarization becomes nearly circular due to differential absorption as the wave enters the ionosphere. The axial ratio of the ellipse is detected with a magnetic dipole antenna in the rocket, connected to a fixed-frequency receiver. The 500 cps modulation signal produced in the output of the rocket receiver is then telemetered to the ground and serves two purposes. First, it is compared with the 500 cps reference frequency which produces the polarization rotation, and the relative phase of these two signals gives the Faraday rotation of the plane of polarization. The second purpose of the 500 cps telemetered signal is to complete the loop of a servomechanism which adjusts the amplitude of the extraordinary circularly polarized signal to keep the modulation level constant at the payload. The amplitude of the 500 cps signal at the rocket tends to decrease due to differential absorption. In terms of polarization, the ellipse tends to approach circularity as differential absorption increases,

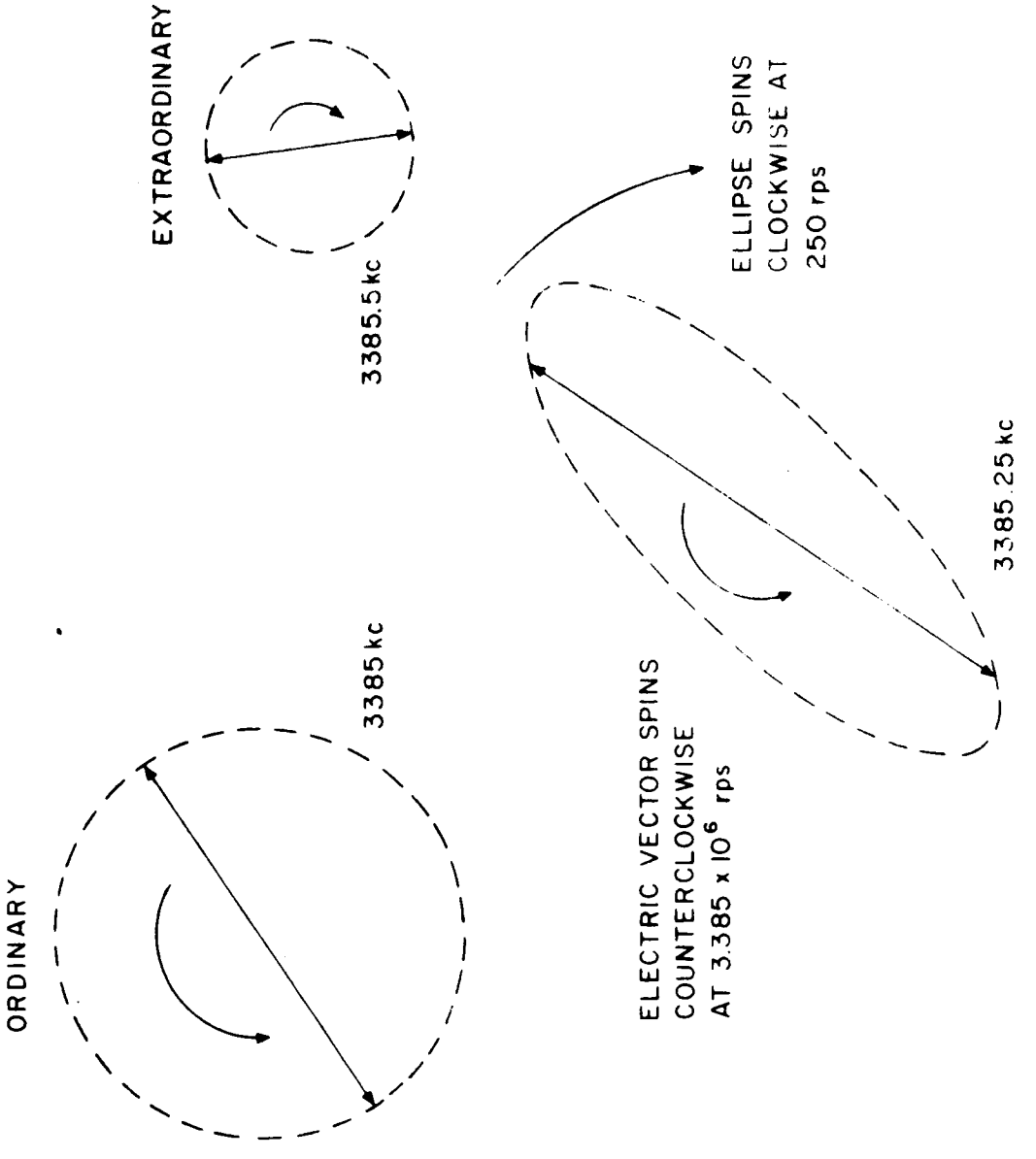

Figure 3.1 Generation of the polarization ellipse.

and the feedback signal controls an attenuator which readjusts the transmitted extraordinary power to keep the axial ratio of the ellipse constant at the rocket. Thus by maintaining the same difference in the intensity between the two wave components received at the rocket, the attenuator settings on the ground give a continuous direct measure of the differential absorption due to the ionosphere.

As noted by Bowhill (1964), radio propagation techniques, in general, possess several advantages over methods of direct measurement of electron density in so far as no perturbations of the ionosphere are produced by the passage of the rocket. With ground-based transmitters and rocket-borne receivers, the payload instrumentation becomes simple with respect to antennas, since small ferrite loops may be used.

The experiment described above yields three parameters, leading to electron density, which can be measured with great accuracy, and which can be used in different altitude ranges. Faraday rotation may be measured in excess of 5000^{o} with an accuracy of 1^{o}, up to the extraordinary wave reflection height (approximately 100 km); differential absorption up to a total of 25 db, with an accuracy of 0.2 db, up to the extraordinary wave reflection height; and ordinary wave refractive index from the standing wave pattern, with 0.05 accuracy, between the reflection heights of the extraordinary and ordinary waves (Bowhill, 1965). These measurements, as will be seen later, yield electron densities from 10 to 10^{5} cm^{-3} over a 100 km altitude range, covering the D- and E-regions of the ionosphere.

3.2 Description of the Ground Station

A block diagram of the experimental system is shown in Figure 3.2 (Knoebel, et al., 1965). The two exciters, designated O and X are crystal-controlled CW oscillators operating at 250 cps above and below the desired center frequency, 2.225 mc or 3.385 mc. The output of each exciter is controlled by a waveguide-beyond-cutoff attenuator, which, in turn, is controlled by the feedback signal from the rocket. In order to obtain circular polarization of the two components, each signal is then passed through a power divider, which distributes the power equally to a variable phase shifter and a variable attenuator. The outputs are added, amplified and then fed to the appropriate antenna. The array consists of four horizontal half-wave dipoles, elevated one-quarter wavelength above the ground. The combined space-and-time quadrature input results in two circularly polarized waves, in opposite senses, corresponding to the ordinary and extraordinary waves. Combining the circular waves with a 500 cps difference results in an elliptically polarized wave, whose plane of polarization rotates at 250 rps.

To assure circularly polarized transmission, a short horizontal ferrite rod antenna is rotated mechanically in the middle of the array. The transmitted modes may then be adjusted independently by means of the phase shifter and attenuator circuits, until circular polarization is obtained.

When the telemetry signal is received from the rocket, it is fed to a modulation discriminator which compares the relative magnitude of

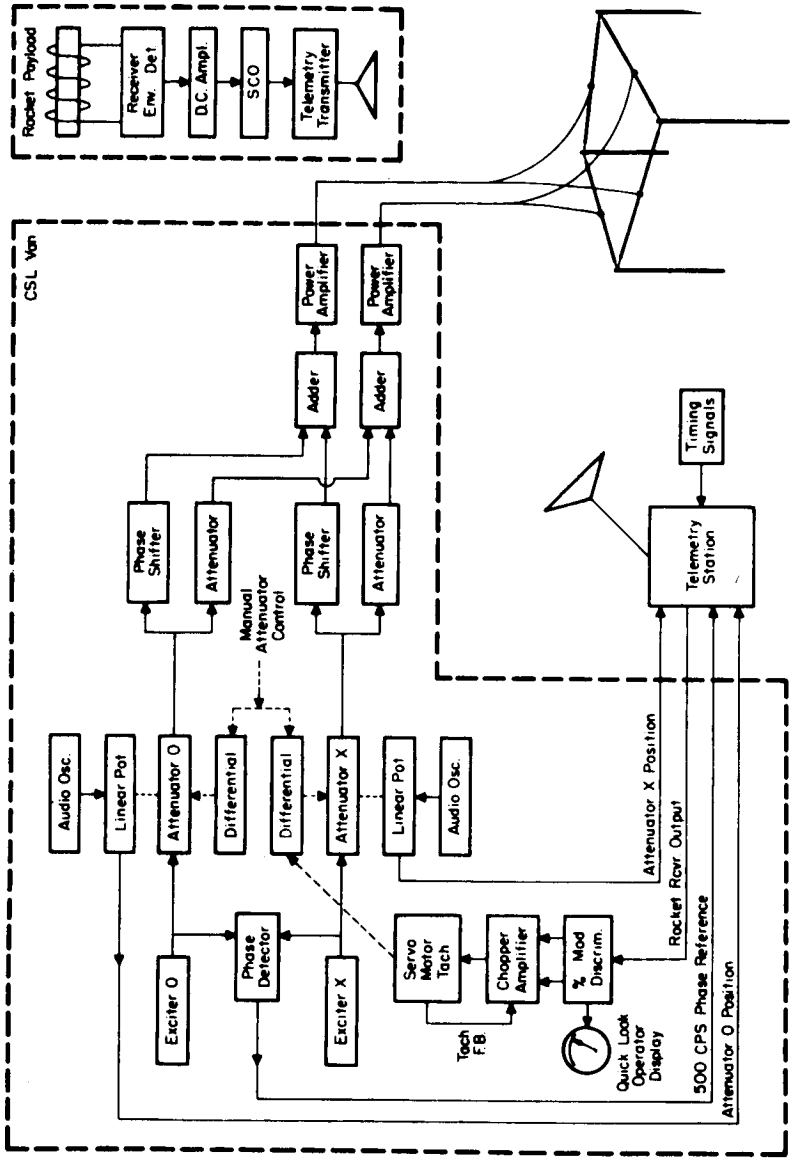

Figure 3.2 Radio propagation experiment system block diagram (after Knoebel et al., 1965).

the ac and dc components of the signal, as a measure of their percent modulation. If this is different from a predetermined value of 32 percent, corresponding to 10 db difference in the intensity of the two waves, a dc error signal is generated and activates a servo motor. The servo motor controls the relative position of the extraordinary wave attenuator, since the ordinary attenuator is left in a constant position, until a constant 32 percent modulation is re-established at the rocket receiver.

In addition to the recording of the various telemetry signals, the 500 cps reference frequency and the attenuator settings, calibrations of the extraordinary and ordinary power, and receiver AGC, are performed and recorded prior, during and after the launch.

3.3 Description of the Rocket Payload

Two types of payload have been launched during the IQSY program. One was designated "Type A", and consisted of the radio propagation experiment, a dc probe, ultraviolet photometers at 1216A^{o} and 1450A^{o}, and solar and magnetic aspect sensors. The probe, photometers and sensors have all been provided by the GCA Corporation. In the other payload, "Type B", the ultraviolet photometers and the solar aspect sensor were replaced by an RF probe, provided by J. Sayers, (University of Birmingham, England), together with either a negatively-biased spherical probe, after K. Hirao and S. Miyazaki, (Radio Research Laboratories, Japan), or a spherical ion trap, provided by A. Nagy, (University of Michigan). Only the Type A payload will be discussed here, since its measurements are needed for the analysis described here.

The radio propagation experiment is described first. Figure 3.3 shows the instrumentation assembly which consists of the ferrite loop antenna, the receiver (at the base), and the tuning network. This part of the payload is enclosed in a fiberglass shell. The ferrite loop antenna is mounted perpendicular to the longitudinal axis of the rocket. It consists of two parallel ferrite rods, wound with a number of turns of insulated wire, depending on the frequency used. The coil is resonated by several capacitors including a trimmer, which permits final tuning of the antenna after the payload is completely assembled. The output of the antenna is fed to a transistorized, crystal-controlled superheterodyne receiver, with a bandwidth of approximately 2 kc, which may be manufactured for operation at 2.225 mc or 3.385 mc. Typical output versus input characteristics of the receiver are shown in Figure 3.4 (Knoebel, et al., 1965).

Figure 3.5 shows the payload shell and the combined instrumentation of the various experiments in the payload. The dc probe experiment (Smith, 1966) consists of the nose tip of the payload, insulated from the remainder of the payload shell which becomes the second electrode. The technique is derived from Langmuir probe theory, and operates in two modes, a fixed and a swept potential. The first measures the current collected by the probe which is held at a constant potential of +2.7 V. In this mode, the electron current is proportional to the electron density, and, as will be shown in the next chapter, the proportionality factor has been found to vary with altitude. The importance of this aspect of the probe measurement lies in the good height resolution

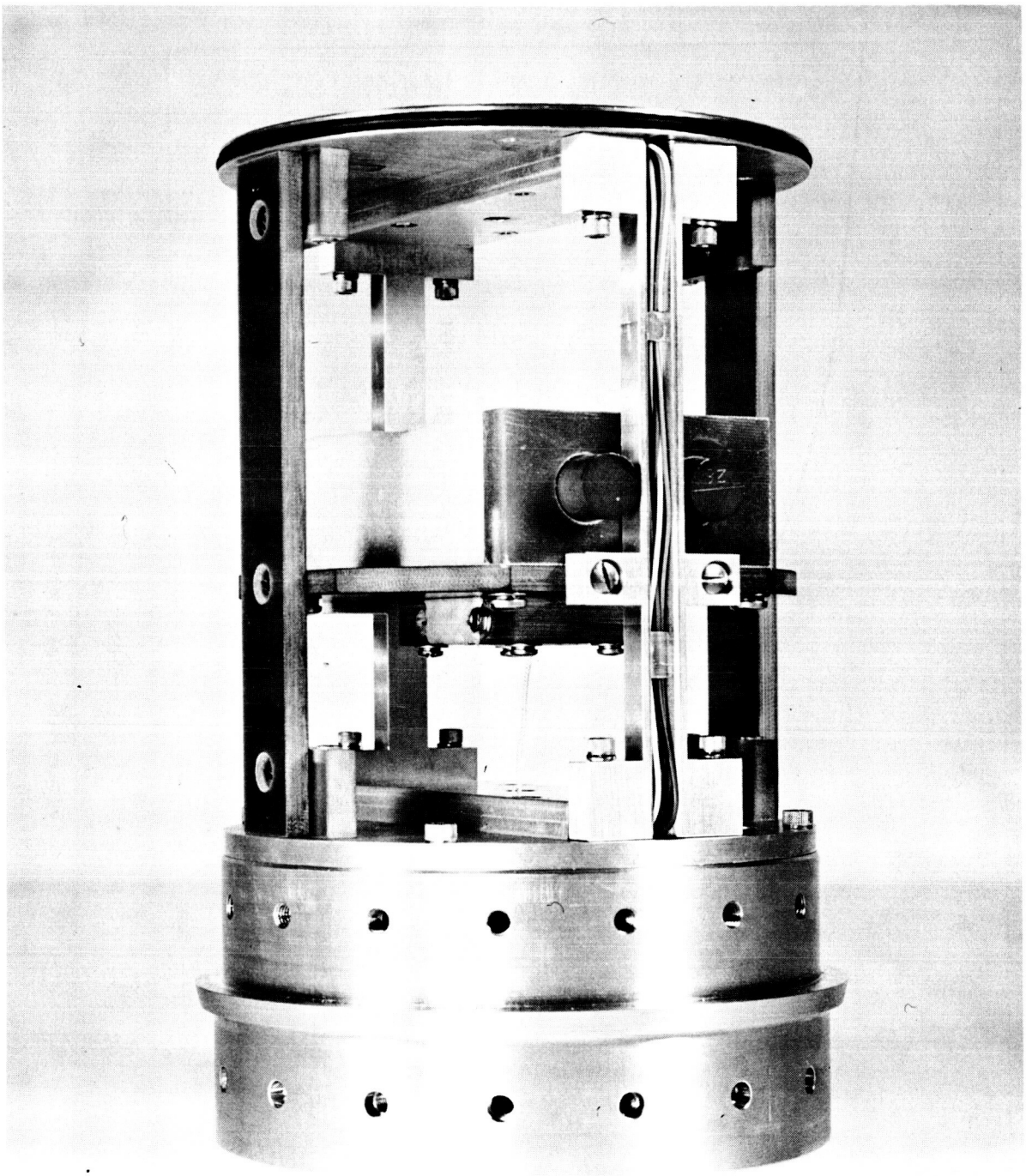

Figure 3.3 Receiver and antenna assembly.

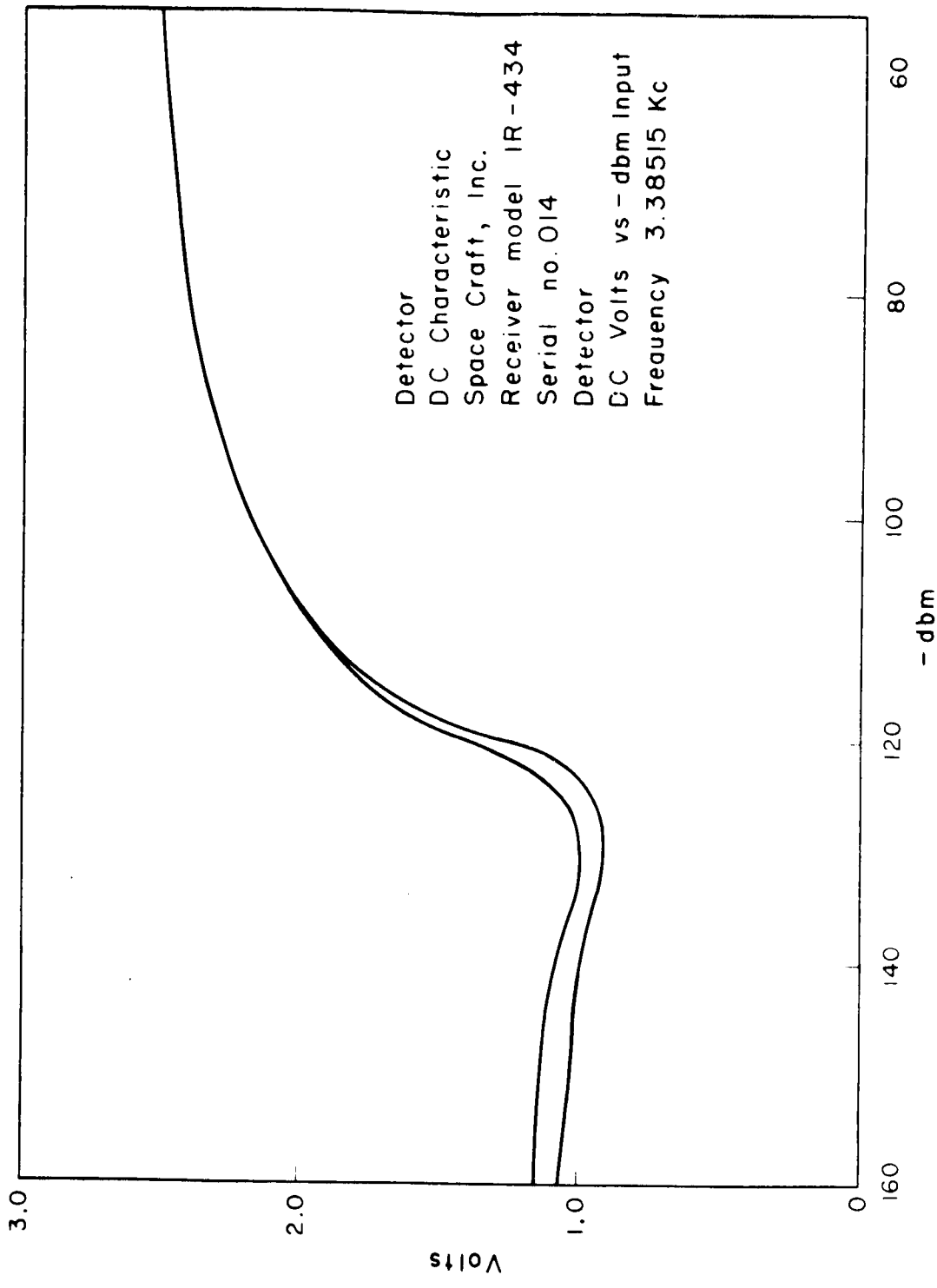

Figure 3.4 Rocket receiver output versus dbm input characteristics (after Knoebel et al., 1965)

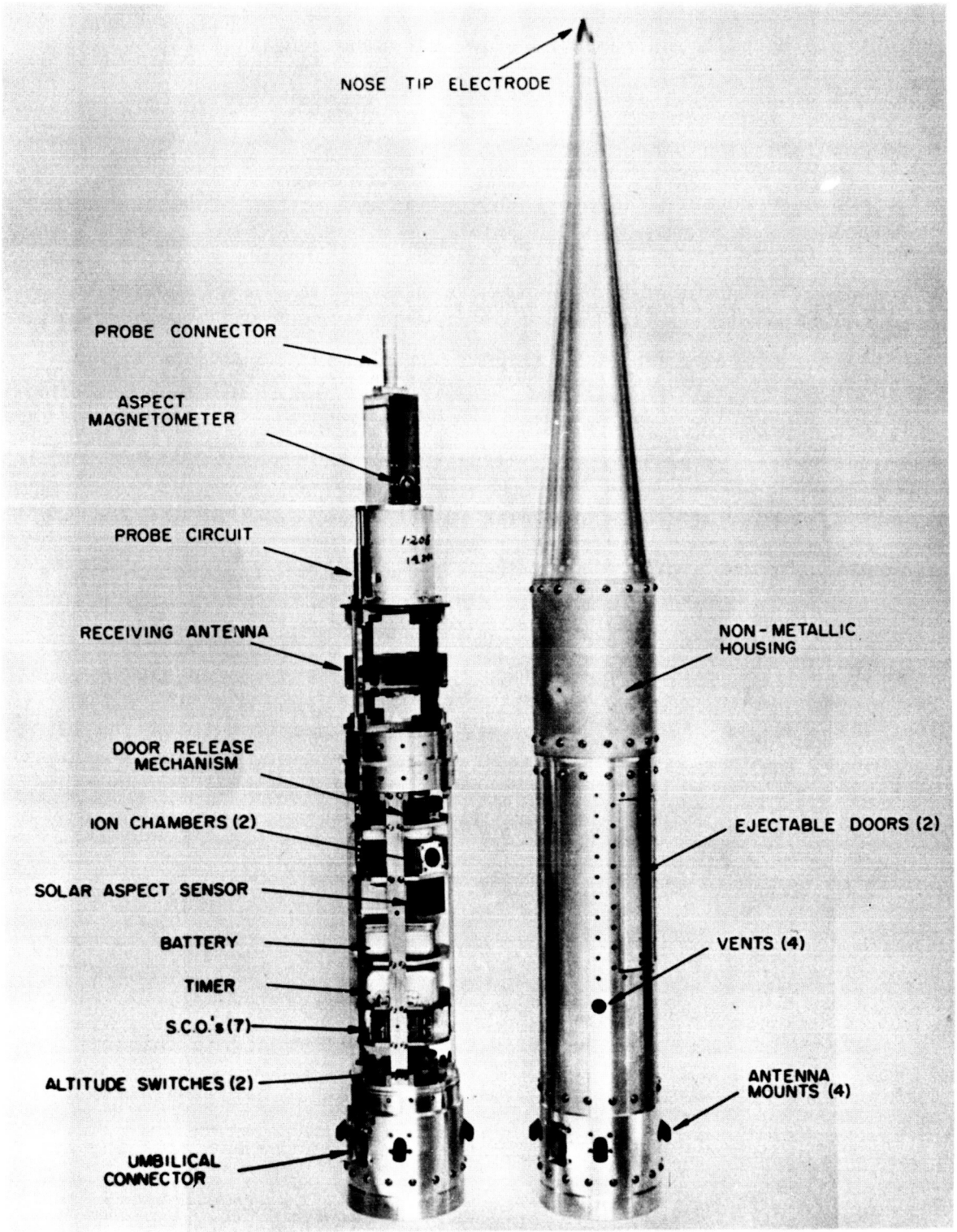

Figure 3.5 Photograph of payload instrumentation and shell.

obtained for the electron current profile. The probe current may then be correlated with the radio measured electron density which possesses absolute accuracy but lacks fine structure resolution. The second mode consists of a sweep, -2.7 V to +2.7 V, applied to the nose tip electrode, to measure the probe current as a function of voltage. By Langmuir theory analysis, the electron density and the electron temperature may be obtained (Smith, 1965). In order to reduce the aspect sensitivity observed on early flights, the shape of the nose tip electrode was changed from a conic to an ogive. Instrumentation details have been given by Smith et al., (1965).

The third important experiment is the measurement of ultraviolet absorption by means of ion chambers. Two types are included in the payload. The first contains nitric oxide at 20 mm pressure and has a 2 mm thick lithium fluoride window; the filling and the window limit the sensitivity of the chamber to a spectral range from 1050A^{o} to 1350A^{o}. Solar flux due to the Lyman-α line at 1216A^{o} is then measured as a function of rocket altitude, and the absorption profile is used to obtain molecular oxygen densities in the D- and lower E-regions of the ionosphere. In addition, the Lyman-α measurement may be used to calculate atmospheric pressure. References to this technique, and methods of analysis are presented in Chapter 5 which is devoted to this experiment. The other ion chamber is sensitive to the spectral band 1425A^{o} to 1480A^{o}, provided by a sapphire window and p-xylene and nitrogen gas fill. It is used primarily to determine molecular oxygen density in

the E-region, and has recently been found capable of measuring the concentration profile of ozone in the D-region (Bowhill and Smith, 1965).

Supporting instrumentation aboard the payload includes a solar aspect sensor which measures the angle at which the ion chambers view the sun.These data are used to correct the response of the ion chambers to condition of normal incidence. Together with the ion chambers, the sensor is protected during launch by doors which are released at an altitude of about 55 km. In addition, a magnetic aspect sensor provides information of vehicle motion, such as spin rate and precession data;and a baroswitch is used to complement radar data to determine the trajectory. An FM/FM telemetry system using seven sub-carrier oscillators has been used to relay the information for the rocket to the ground.

3.4 Reduction of the Radio Propagation Data

The most important feature of the radio propagation experimental system described in Section 3.1, is its ability to measure Faraday rotation and differential absorption with high resolution. The need for an accurate, high sampling rate of the measured data demands an automatic and computerized reduction system. Such a system will now be desribed.

To measure differential absorption, magnetic tape information containing the extraordinary and attenuator monitor voltage and time signals is transferred to an analog-to-digital recorder at one-sixteenth speed of original recording. A synchronizer unit then sends these signals in the form of command pulses to an analog-digital converter,

which punches the data in binary form. The punched paper tape is then fed to a digital computer which prints and plots the extraordinary attenuator settings versus time. Since the data are sampled at 100 points per sec, median and average values are also calculated. Typical computer plotted attenuator settings, marked extraordinary power, are shown in Figure 3.6, where the absorption spikes at 63, 68, and 83 sec after launch are due to magnetic tape dropouts and should be dismissed. The data beyond the extraordinary reflection height at 104 km, corresponding to 86 sec after launch, are meaningless. Since the ordinary power is kept constant throughout the experiment, (20 db for the flight shown in Fig. 3.6), the differential absorption may be easily computed. Later, it will be shown that only the rate of change of differential absorption is needed, and therefore the extraordinary power values suffice for the calculation of electron density.

The reduction of the Faraday rotation data is more complex. The recorded information, from which it is extracted, contains the sum of the 500 cps reference frequency, twice the rocket spin and twice the contribution of the Faraday rotation. In order to separate these signals, the ground-transmitted wave reference angle (500 cps) is fed to a mechanical phase shifter, whose servo-driven shaft position indicates twice the Faraday rotation angle. To generate this shaft position, the following feedback loop is used (Gooch, 1965). The mechanical phase shifter output is added, in a polyphase heterodyne system, to twice the rocket roll which is obtained independently from the magnetic aspect sensor. This forms a relatively noise-free and sinusoidal synthesized

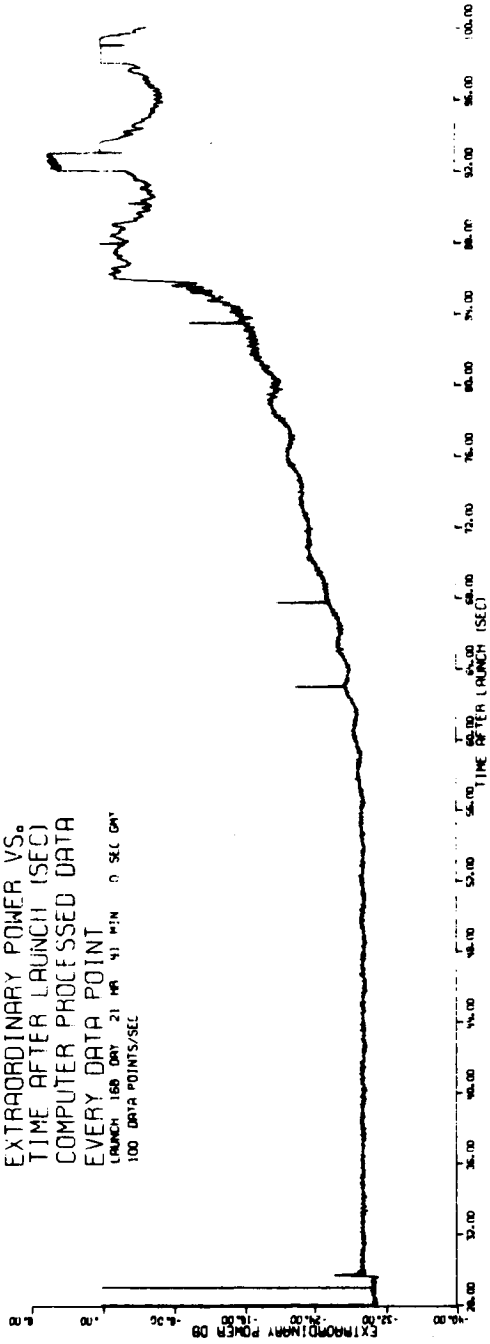

Figure 3.6 Extraordinary power versus time after launch.

sum reference which may be compared to the rocket receiver signal. In the case of the Southern hemisphere launches, the rocket roll is subtracted, since the ground wave is transmitted in opposite sense to that in the Northern hemisphere. By comparing the synthesized reference signal to the rocket receiver signal by means of a pulse detector, a polarized servo-error signal is produced. The error signal tends to zero when the two signals are in phase quadrature. When they are not, the error signal excites a servo motor which is mechanically coupled to the phase shifter. The shaft revolutions are geared to a multi-turn potentiometer which yields Faraday rotation data at 0.0001 volts per degree. This, in turn, is fed to an integrating digital voltmeter which punches the data on paper tape, together with timing marks. A digital computer finally prints and plots the data. A typical example is shown in Figure 3.7.

The procedure for reducing the Faraday rotation data to electron density, and the method of extracting a collision frequency model from the differential absorption, are the subject of the following chapter.

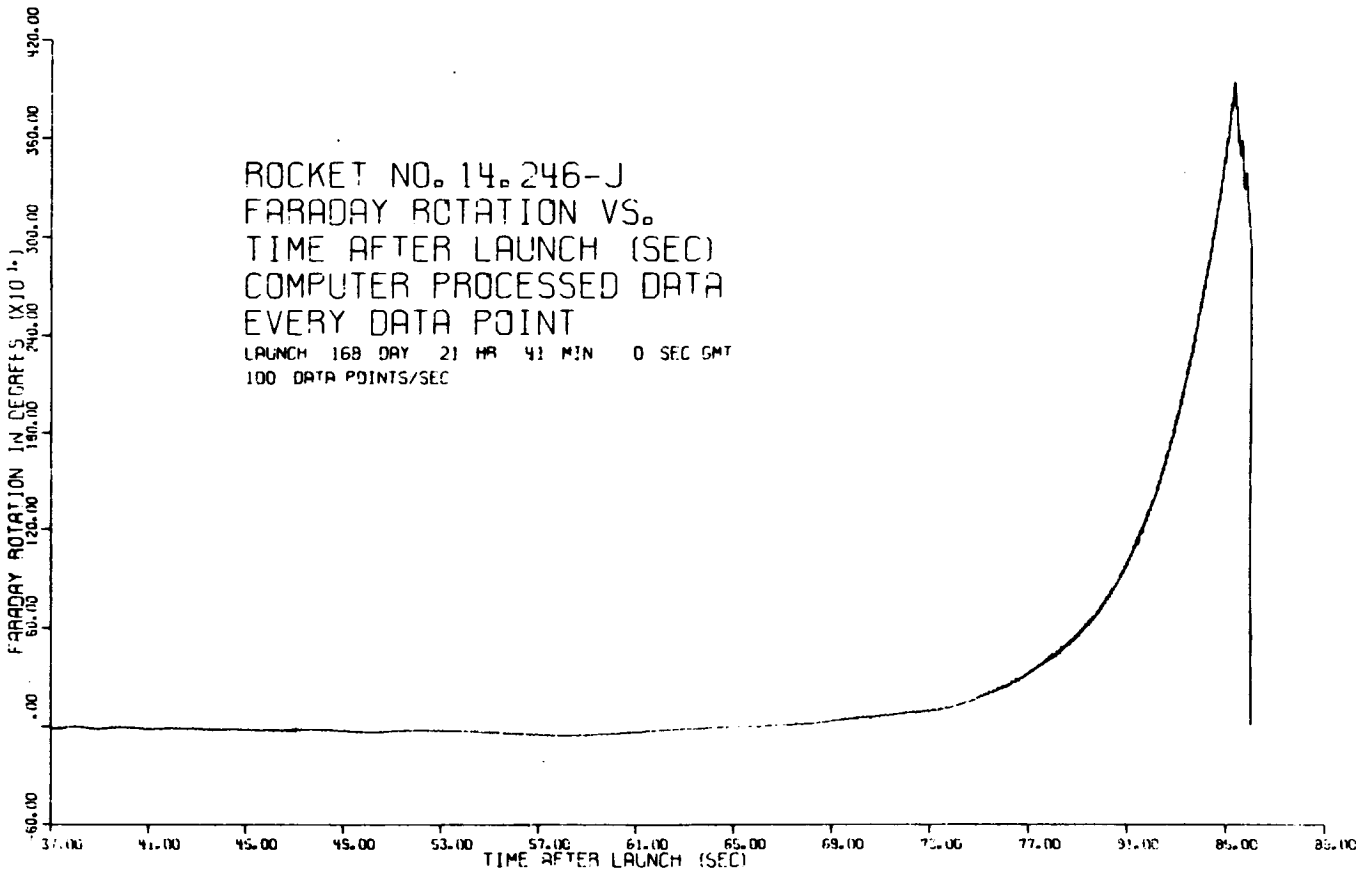

Figure 3.7 Faraday rotation versus time after launch.

4. METHODS OF OBTAINING ELECTRON DENSITY PROFILES AND COLLISION FREQUENCY MODELS FROM THE EXPERIMENTAL DATA

In this chapter, the methods of analysis of the experimental radio propagation data are described in detail. From the expression for the phase refractive index derived in Section 2.2, a formula is developed for the calculation of electron densities from the Faraday rotation measurements. Similarly, from the expression for the absorption coefficient, and from the knowledge of electron density, an analytical method is derived to determine the electron collision frequency from the differential absorption measurements.

However, as explained in Section 2.1, since the frequency of propagation exceeds the gyrofrequency, the extraordinary wave is reflected at $X = 1 - Y$, which corresponds usually to a daytime altitude of about 100 km for frequencies in the range 2 to 4 mc. Therefore, above the extraordinary reflection height, differential absorption and Faraday rotation cannot be measured. The ordinary wave, however, penetrates farther into the ionosphere and is reflected when $X = 1$, which corresponds to an altitude at the base of the F-layer. Above the extraordinary reflection height, the electron density is then obtained from the ordinary phase refractive index. This is determined from the analysis of the standing wave pattern produced at the rocket by a direct ordinary wave and a wave reflected from the F-layer.

At low altitudes, below 80 km, where Faraday rotation is very small, and where the dc probe measurements of electron current tend to overestimate the electron density, the collision frequency model is

extrapolated to these altitudes and a range of electron densities is calculated from the absorption measurements.

These analytical methods are described, and results of their application to several rocket flights are presented. The correlation between the electron density measured by the radio propagation technique and the electron current measured by the dc probe is also given, together with a general comparison of the measured electron collision frequencies.

4.1 Electron Density from Faraday Rotation Measurements

Faraday rotation has been defined as the angle of rotation of the electric field vector after passage through an ionization slab. It is measured by the relative change in the phase refractive index of the two magneto-ionic modes. Assuming straight line propagation, and according to the resultant field expressed in Equation (2.28), the phase of the ordinary wave, ϕ_o, may be written as

$$\phi_o = \frac{2\pi}{\lambda_o} \int_o^h \mu_o \, ds \ . \tag{4.1}$$

where λ_o is the propagation wavelength in free space, μ_o is the ordinary phase refractive index, and s is the distance along the propagation path. Similarly, the phase of the extraordinary wave, ϕ_x, may be written as

$$\phi_x = \frac{2\pi}{\lambda_o} \int_o^h \mu_x \, ds \ , \tag{4.2}$$

where μ_x is the extraordinary wave phase refractive index. The phase difference is then given by

$$\phi_o - \phi_x = \frac{2\pi}{\lambda_o} \int_o^h (\mu_o - \mu_x)\, ds \ . \tag{4.3}$$

It can be easily seen that if the extraordinary phase changes by an angle ψ, the resultant phase of the ordinary and extraordinary waves changes by $\frac{\psi}{2}$. Therefore the Faraday rotation angle, ϕ, is defined by half the phase difference between the ordinary and extraordinary waves, and is given by

$$\phi = \frac{\pi}{\lambda_o} \int_o^h (\mu_o - \mu_x)\, ds \ . \tag{4.4}$$

Assuming that the rocket travels along the ray path, an angle of elevation, θ, may be defined between the path and the ground plane. The path differential ds may then be expressed by

$$ds = dz \ \text{cosec}\ \theta \ , \tag{4.5}$$

where z is the altitude measured vertically upwards. Substituting Equation (4.5) in Equation (4.4) and assuming θ is constant, the rate of change of Faraday rotation may be written as

$$\frac{d\phi}{dt} = \frac{\pi}{\lambda_o} \ \text{cosec}\ \theta \ \frac{dz}{dt} \ (\mu_o - \mu_x) \ , \tag{4.6}$$

where $\frac{dz}{dt}$ is the velocity of the rocket in the z-direction, V_z. Hence V_z cosec θ is the velocity of the rocket along the propagation path. Equation (4.6) is then written as

$$\frac{d\phi}{dt} = \frac{\pi}{\lambda_o} V_z \text{ cosec } \theta \, (\mu_o - \mu_x) \, . \tag{4.7}$$

The phase refractive index has been derived in Section 2.2 for the quasi-longitudinal approximation, and Equation (2.24) may be expressed as

$$\mu_o = 1 - \frac{\frac{1}{2} X \, (1 + Y_L)}{(1 + Y_L)^2 + Z^2} \, , \tag{4.8}$$

and

$$\mu_o = 1 - \frac{\frac{1}{2} X \, (1 - Y_L)}{(1 - Y_L)^2 + Z^2} \, . \tag{4.9}$$

The quantity $\mu_o - \mu_x$ is then calculated, and after several algebraic manipulations the result is expressed by

$$\mu_o - \mu_x = \frac{XY_L \, (1 - Y_L^2 - Z^2)}{[(1+Y_L)^2 + Z^2][(1-Y_L)^2 + Z^2]} \, . \tag{4.10}$$

For altitudes above 75 km, where the collision frequency is smaller than the propagation frequency, or $Z \ll 1$, the term Z^2 may be neglected.

This simplifies Equation (4.10) to

$$\mu_o - \mu_x = \frac{XY_L}{1 - Y_L^2} \quad . \tag{4.11}$$

Substituting Equation (4.11) in Equation (4.7) and solving for X, the following expression is obtained

$$X = \frac{1-Y_L^2}{Y_L} \quad \frac{\lambda_o}{\pi} \quad \frac{\sin\theta}{V_z} \quad \frac{d\phi}{dt} \quad . \tag{4.12}$$

The symbol X has been defined by Equation (2.9) as

$$X = \frac{Ne^2}{\varepsilon_o m\omega^2} \quad . \tag{4.13}$$

Substituting the value for X in Equation (4.12) and solving for N, we obtain

$$N = \frac{\varepsilon_o m\omega^2}{e^2} \quad \frac{1-Y_L^2}{Y_L} \quad \frac{\lambda_o}{\pi} \quad \frac{\sin\theta}{V_z} \quad \frac{d\phi}{dt} \quad . \tag{4.14}$$

A simplified form of Equation (4.14) is obtained when the values for the various constants are substituted, thus

$$N = R \frac{d\phi}{dt} \tag{4.15}$$

where

$$R = 20.66\ f\ \frac{1-Y_L^2}{Y_L}\ \frac{\sin\theta}{V_z}\ , \qquad (4.16)$$

and where f is expressed in mc, V_z in the km sec^{-1} and N is obtained in cm^{-3}. The parameters θ and V_z are determined from the radar trajectory of the rocket. The Faraday rotation is measured experimentally, and $\frac{d\phi}{dt}$ may be easily calculated from the automatically processed data described in Section 3.4. The parameter Y_L is computed from the earth's magnetic field which is determined by means of a Fortran computer program (Eckhouse, 1964). A spherical harmonic expansion using Gaussian coefficients is used, and the input includes geographic positions and various trajectory parameters.

This technique for the measurement of electron density is relatively simple and accurate. The measurement of Faraday rotation is obtained in an unambiguous manner, and most of the difficulties associated with the same measurement from satellites, as discussed by Bowhill and Schmerling (1961), are alleviated. The angle of rotation is measured with an accuracy of 1^o, but the final height resolution of the electron density is limited to 1 km. The upper altitude limit for the electron density obtained by this technique is the height of reflection of the extraordinary wave, since no Faraday rotation can be measured above that altitude. The results of the Faraday rotation measurements for several rocket flights are presented at the end of the chapter.

4.2 Determination of the Electron Collision Frequency from Absorption Measurements

It has been shown in Section 2.2 that the absorption of radio waves in an ionized medium depends on the frequency with which electrons collide with heavy particles. The absorption may then be used to give an estimate of this collision frequency.

From the Appleton-Hartree formula, Equation (2.25) has been developed for the imaginary part, χ, of the refractive index and may be expressed as

$$\chi_x = \frac{\frac{1}{2} XZ}{(1-Y_L)^2+Z^2} \quad , \tag{4.17}$$

and

$$\chi_o = \frac{\frac{1}{2} XZ}{(1+Y_L)^2+Z^2} \quad . \tag{4.18}$$

From the resultant electric field expressed in Equation (2.28), the differential absorption, in nepers, is given by

$$\ln A = \frac{2\pi}{\lambda_o} \int_o^h (\chi_x - \chi_o)\, ds \quad . \tag{4.19}$$

Neglecting collisions, and replacing the quantity $\chi_x - \chi_o$ by the difference of the two expressions given by Equations (4.17) and (4.18), the rate of absorption, in decibels, is

$$\frac{d(\ln A)}{dt} = \frac{2\pi}{\lambda_o} (8.69) (\chi_x - \chi_o) \frac{ds}{dt} , \tag{4.20}$$

$$= \frac{2\pi}{\lambda_o} (8.69) \frac{2 X Z Y_L}{(1-Y_L^2)^2} \frac{ds}{dt} , \tag{4.21}$$

$$= \frac{4\pi}{\lambda_o} (8.69) \frac{V_z \operatorname{cosec} \theta Y_L}{(1-Y_L^2)^2} XZ . \tag{4.22}$$

Examination of Equation (4.22) shows that the rate of change of differential absorption is proportional to the product $N\nu$ as represented by the product XZ. The electron density, however, is known from the Faraday rotation measurements, and therefore it is possible to extract ν from Equation (4.22). For this purpose, we calculate the ratio of the rate of absorption to the rate of Faraday rotation, obtained from Equations (4.12) and (4.22), thus

$$\frac{d(\ln A) / dt}{d\phi / dt} = \frac{4\pi \times 8.69}{180} \frac{Z}{1-Y_L^2} . \tag{4.23}$$

Since $Z = \frac{\nu}{\omega}$, then Equation (4.23) may be written as

$$\frac{d(\ln A) / dt}{d\phi / dt} = k_1 \nu , \tag{4.24}$$

where

$$k_1 = \frac{1}{10.36 f (1-Y_L^2)} . \tag{4.25}$$

The electron collision frequency, as derived from the Appleton-Hartree formula may now be taken directly proportional to the air pressure, P, thus

$$\nu_{AH} = k_2 P \ . \tag{4.26}$$

When the value of k_2 is found, it is convenient to refer to Equation (4.26) as the collision frequency model in a certain altitude range for a particular rocket flight. Substituting Equation (4.26) in Equation (4.24), transposing the ratio, and integrating by parts we obtain

$$\ln A = k_1 k_2 \left(\phi P - \int_o^z \phi \frac{dP}{dt} \, dt\right) \tag{4.27}$$

Moreover, the hydrostatic equation for the neutral atmosphere gives

$$\frac{dP}{dz} = \frac{-P}{H} \ , \tag{4.28}$$

where H is the scale height defined by

$$H = \frac{kT}{mg} \ , \tag{4.29}$$

and k is Boltzmann's constant, T is the temperature, m is the mean molecular mass, and g is the acceleration due to gravity. Introducing $V_z = \frac{dz}{dt}$ in Equation (4.28), we obtain

$$\frac{dP}{dt} = - \frac{P}{H} V_z \quad . \tag{4.30}$$

Substitution of Equation (4.30) in Equation (4.27) results in

$$\ln A = k_1 k_2 \left(\phi P + \int_o^z \frac{\phi P V_z}{H} \, dt\right) \quad . \tag{4.31}$$

The term ln A represents the total differential absorption of the two propagated waves. This relative absorption consists of the deviative and the non-deviative absorption. Deviative absorption occurs near the level of reflection and whenever there is marked bending of the ray as the phase refractive index approaches zero. Non-deviative absorption occurs in the D-region of the ionosphere, where the product $N\nu$ is large, and where the phase refractive index is near unity. In order to apply the absorption measurements to the D-region, it is then necessary to correct for the deviative type of absorption. When the imaginary parts of Equation (2.18) are equated and Z^2 in the denominator set to be zero, we obtain

$$\chi_{o,x} = \frac{\frac{1}{2} X Z}{(1 \pm Y_L)^2} \frac{1}{\mu_{o,x}} \tag{4.32}$$

The difference in attenuation may then be expressed as

$$\chi_x - \chi_o = \frac{\frac{1}{2} X Z}{(1-Y_L^2)^2} \left\{ \frac{(1+Y_L)^2}{\mu_x} - \frac{(1-Y_L)^2}{\mu_o} \right\} \tag{4.33}$$

$$= \frac{2 X Z}{(1-Y_L^2)^2} \left\{ \frac{1}{4} \frac{(1+Y_L)^2}{Y_L} \frac{1}{\mu_x} - \frac{1}{4} \frac{(1-Y_L)^2}{Y_L} \frac{1}{\mu_o} \right\} \tag{4.34}$$

It should be noted that Equation (4.34) reduces to the non-deviative form expressed in Equations (4.10) and (4.18) where μ_x and μ_o equal one. Therefore a correction factor of the form

$$\gamma = \frac{1}{\frac{1}{4} \frac{(1+Y_L)^2}{Y_L} \frac{1}{\mu_x} - \frac{(1-Y_L)^2}{Y_L} \frac{1}{\mu_o}} , \tag{4.35}$$

may be applied to the total absorption to yield the non-deviative absorption, represented by $\ln A_n$. The phase refractive indices may be deduced from the Faraday rotation electron density by

$$\mu_{o,x} = \sqrt{1 - \frac{X}{1 \pm Y_L}} . \tag{4.36}$$

Figure 4.1 shows γ as a function of electron density. As the extraordinary wave approaches the level of reflection, μ_x and γ approach zero.

When $\ln A_n$ is substituted for $\ln A$ in Equation (4.31), and plotted

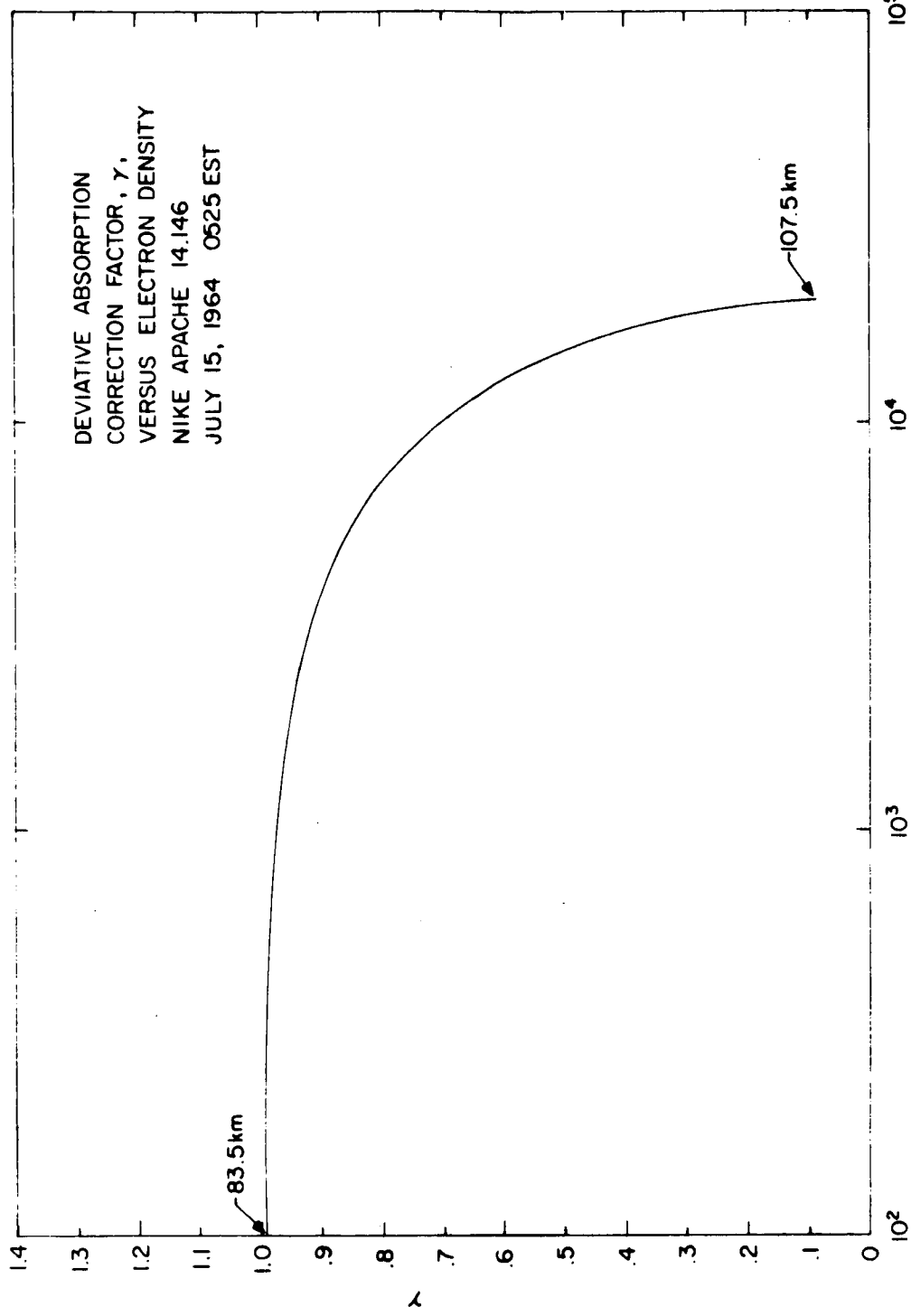

Figure 4.1 Deviative absorption correction factor versus electron density.

versus

$$\phi P + \int_o^z \frac{\phi P}{H} V_z \, dt \ ,$$

the value of $k_1 k_2$ may be obtained from the smoothed slope of

$$\frac{\Delta (\ln A)}{\Delta \left(\phi P + \int_o^z \frac{\phi P}{H} V_z \, dt \right)} \ .$$

Since k_1 is given by Equation (4.25), then k_2 may be computed and the collision frequency model is finally obtained. The electron collision frequency thus deduced is assumed to be independent of electron velocity. In the treatment of the generalized Appleton-Hartree formulas in Section 2.3, it was shown that when ν_{AH} is associated with the mean energy, improved agreement is obtained between the Appleton-Hartree theory and the generalized theory. In the D-region and above, the collision frequency is much smaller than the propagation frequency (greater than 2mc for our experiment), and in this asymptotic limit, $\nu_{AH} = \frac{5}{2} \nu_m$, where ν_m is the collision frequency for monoenergetic electrons (Sen and Wyller, 1960). Comparison of the collision frequency models deduced from the absorption for various rocket flights will be presented at the end of this chapter.

4.3 Electron Density from Differential Absorption Measurements

In order to check the validity of the electron collision frequency model derived from the absorption data, the electron density should be

re-evaluated using the differential absorption information. This electron density should match the electron density computed from Faraday rotation, since the latter values were used to extract the collision frequency model.

Solving for X in Equation (4.22) we obtain

$$X = \frac{\lambda_o}{4\pi \times 8.69 \times V_z \operatorname{cosec}\theta} \frac{1-Y_L^2}{Y_L} \frac{1}{Z} \frac{d}{dt} (\ln A) \quad . \tag{4.37}$$

By substituting the values for the various symbols and constants in Equation (4.37), the electron density is given by

$$N = \rho \frac{1}{P} \frac{d(\ln A)}{dt} \quad , \tag{4.38}$$

where

$$\rho = \frac{2.14 \times 10^8 f^2}{k_2} \frac{\sin\theta}{V_Z} \frac{(1-Y_L^2)^2}{Y_L} \quad , \tag{4.39}$$

and where k_2 is the collision frequency model constant, f is expressed in mc, P in mm of mercury, V_z in km sec^{-1}, and N is obtained in cm^{-3}.

If the electron densities calculated by Equations (4.38) and (4.39) agree with those obtained from the Faraday rotation, then the derived collision frequency model is correct. For the electron density profiles shown in Section 4.5, the densities derived by differential absorption

are superimposed on the Faraday rotation results, and they are seen to agree satisfactorily.

The collision frequency model obtained by the method outlined in Section 4.2 applies in the same range as the Faraday rotation and differential absorption measurements, and is limited at the upper altitude by the extraordinary reflection height. This collision frequency model, however, may be extrapolated to lower altitudes where the differential absorption and the dc probe electron current, I, may be used to provide a range of electron densities. Below 80 km, the electron current tends to overestimate the electron density, whereas above that altitude, it gives a good measure of the density, as will be shown in Section 4.5. Therefore if the differential absorption is plotted versus $\int_o^z PI ds$, where the latter quantity represents $\int_o^z \nu N ds$, it is possible to obtain the ratio of electron density to electron current, and to compute a range of electron densities at these altitudes. Thus

$$S_1 = \frac{\Delta(\ln A)}{\Delta \int_o^h PI ds} = \frac{\Delta(\ln A)}{\Delta \int_o^t PIV_z \operatorname{cosec}\theta \, dt} , \tag{4.40}$$

provides a constant slope obtained by drawing a straight line through the scattered points, and S_2 is a slope obtained at each point. Equation (4.38) may be expressed as

$$\frac{d(\ln A)}{dt} = \frac{1}{\rho} NP , \tag{4.41}$$

and the electron density is then given by

$$N = S_{1,2} \rho I \quad . \tag{4.42}$$

The two slopes S_1 and S_2 provide the two limits in the range of densities obtained by this method. The accuracy of this technique depends on whether the differential absorption is measured with enough resolution at these altitudes, and whether the dc probe measurements at these altitudes are dependable. An estimated 25% probable error may be attached to the range of densities thus obtained, because of the smoothing involved in the procedure of computing slopes, and due to the extrapolation of the collision frequency model. Despite this uncertainty, the technique described above is valuable since otherwise, no measure of the electron density at these altitudes may be obtained from the radio propagation data. Some of the ranges of electron density are shown in Section 4.5.

4.4 Electron Density by Standing Wave Analysis

The Faraday rotation and differential absorption methods described in the previous sections provide electron densities up to the extraordinary reflection height. The ordinary wave, however, penetrates farther into the ionosphere and is reflected when X = 1. This corresponds to an altitude in the F-region, where the electron density is large enough to satisfy the reflection condition. The following analysis describes the method used to obtain the ordinary phase refractive index, and therefore the electron density, from the standing wave pattern produced at the rocket by a direct and a reflected ordinary wave. An

isotropic, horizontally stratified medium is assumed and the effect of the curvature of the earth is neglected.

Consider the geometry of the various paths drawn in Figure 4.2, where S represents the rocket path, p the propagation path, Δp an increase in the propagated wave path, and Δr a decrease in the reflected wave path. The quantity $(\Delta p - \Delta r)$ represents an increase in path difference, and the rate of this increase is a function of the maxima in the standing wave pattern. The standing wave pattern is observed superimposed on the output of the rocket receiver which is printed with high resolution on telemetry charts. The rate of path difference may be calculated from the trajectory in the following manner. Consider a direct ordinary wave that has penetrated the E-layer and has reached an altitude z which corresponds to the position of the rocket. The path length of this direct wave, given by b in Figure 4.3, represents the slant range of the rocket, and the angle of the propagation wave, θ, is the elevation angle of the trajectory. Another direct wave reaches a height h, where the condition for reflection is satisfied, and is reflected down to meet the direct wave at the rocket. These two vectors, the direct and reflected waves, add to form a standing wave which is projected along the path of the rocket. The height h may be obtained from an ionogram taken at the time of the flight, after appropriate corrections are made for conversion from virtual to real height. Moreover, the refractive properties of the ionosphere cause the penetrating ray to bend as it propagates. However, by the Breit and Tuve theorem (Budden, 1961), a triangulated path is a valid approximation to associate with the exact ray path.

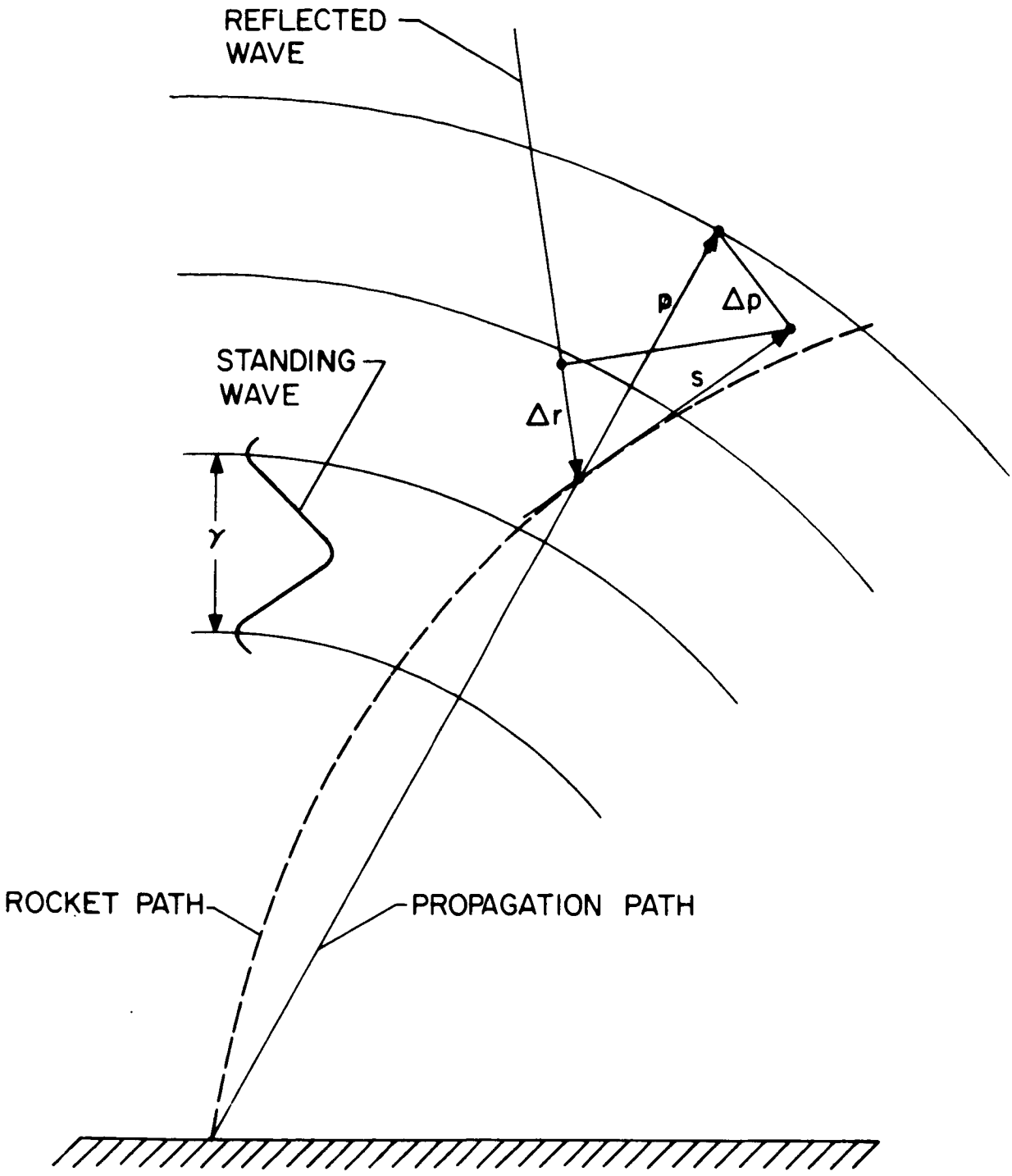

Figure 4.2 Geometry of ray paths for standing wave analysis.

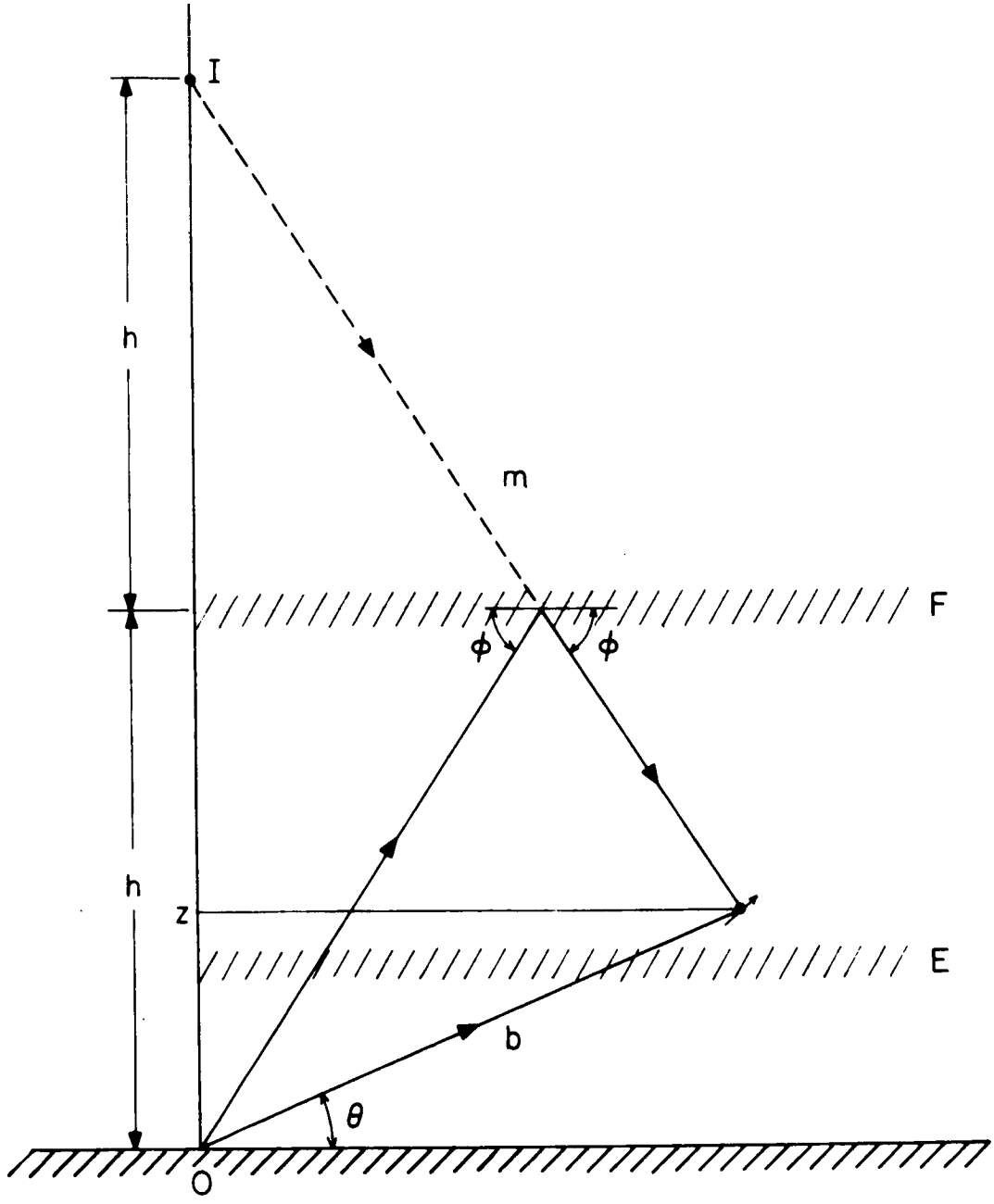

Figure 4.3 Geometry for the computation of path difference from rocket trajectory.

This is shown in Figure 4.3. Therefore, since the wave is reflected at an angle equal to the incidence angle, the reflected wave may be assumed to have originated at a mirror point I, at an altitude of 2h. Then by the cosine law,

$$m^2 = 4h^2 + b^2 - 4hb \sin\theta \tag{4.43}$$

Differentiating with respect to time, and subtracting $\frac{db}{dt}$ from both sides, we obtain

$$\frac{db}{dr} - \frac{dm}{dr} = \left(1 + \frac{2h}{m} \sin\theta - \frac{b}{m}\right)\frac{db}{dt} + \frac{2hb}{m}\cos\theta \frac{d\theta}{dt} \quad . \tag{4.44}$$

The quantity $\left(\frac{db}{dt} - \frac{dm}{dt}\right)$ is equivalent to the rate of change in path difference. The ordinary phase refractive index, μ_o, under the assumptions presented above, is given by

$$\mu_o = \frac{\lambda_o}{\lambda} \quad , \tag{4.45}$$

where λ is the wavelength in the medium and λ_o is the wavelength in free space. This ratio may be given by

$$\mu_o = \frac{\lambda_o}{\lambda} = \frac{\frac{d(sw)}{dt} \Big/ \dot{\lambda}}{\left(\frac{db}{dr} - \frac{dm}{dr}\right) \Big/ \lambda_o} \quad , \tag{4.46}$$

where $\frac{d(sw)}{dt} \Big/ \lambda$ represents the number of standing wave maxima per second counted on the receiver output telemetry chart. The quantity $\left(\frac{db}{dt} - \frac{dm}{dt}\right) \Big/ \lambda_o$ may be evaluated for each corresponding altitude and μ_o can then be found as a function of height. For $Z << 1$, the ordinary phase refractive index has been given in Equation (4.8) by

$$\mu_o = 1 - \frac{\frac{1}{2} X}{1+Y_L} \quad . \tag{4.47}$$

Then, solving for X and substituting the values of the symbols and constants, we obtain an expression for electron density in cm^{-3}

$$N = 1.24 \times 10^4 f^2 (1 + Y_L) (1 - \mu_o^2) \quad , \tag{4.48}$$

where f is in mc.

The main difficulty in the analysis presented above is the counting of the standing wave maxima superimposed on the receiver output. Often, this output becomes noisy at the higher altitudes and the interference pattern is not easily resolved. Several criteria have been set for cycle counting in order to take account of possible phase reversals, but the uncertainty in the results of several rocket flights exceeds an estimated probable error of 20%.

In general, the electron density derived by the standing wave analysis agreed satisfactorily with the electron current profile measured by the dc probe. It will be seen from the results of the next section that in the region above 100 km, there is almost exact

proportionality between the electron current and the electron density. The electron density computed by this method has also been used to obtain an aspect correction for the probe current at these altitudes, as will be shown for rocket flight 14.146.

4.5 Sample Results and Correlation with Electron Current

In a forthcoming report by Salah and Bowhill (1966), the details involved in the various analysis techniques, and the electron densities and collision frequencies measured by the rockets during the International Quiet Sun Years will be presented. In the present work, however, a sample of the results will be given to illustrate the application of the various methods described in the preceeding sections. Table 4.1 gives some of the relevant data describing the rocket flights whose results will be given here.

The series of rocket flights 14.144, 14.145, and 14.146 was launched to study the role of photodetachment in the lower D-region of the ionosphere and the structure changes of the ionosphere from night to daytime (Bowhill and Smith, 1965). The first rocket was launched before layer sunrise, when no visible radiation was incident on the layer; the second was launched after layer sunrise but before ground sunrise when only visible radiation was present in the D-region; the third rocket was launched after ground sunrise. The series 14.230, 14.231, and 14.232 was a part of a five rocket series launched from aboard NASA's mobile carrier, USNS CROATAN, in the southern hemisphere, to study the latitudinal variations in electron density. Flight 14.246

Flight Number	Date of Launch	Time of Launch	Solar Zenith Angle	Geographic Position	Propagation Frequency
14.144	15 July 1964	0300:00 EST	105°	Wallops Island, Va.*	2.225 mc
14.145	15 July 1964	0420:00 EST	96°	Wallops Island, Va.	2.225 mc
14.146	15 July 1964	0520:00 EST	85°	Wallops Island, Va.	2.225 mc
14.230	5 April 1965	0845:53 EST	58°	29°34'S, 75°13'W	3.385 mc
14.231	9 April 1965	1418:15 EST	60°	44°15'S, 77°40'W	3.385 mc
14.232	12 April 1965	1214:02 EST	67°	58°19'S, 78° W	3.385 mc
14.246	17 June 1964	1641:00 EST	60°	Wallops Island, Va.	3.385 mc

*Wallops Island, Va. :37° 50'N, 75° 29'W

Table 4.1 Launch data for several rocket flights.

was launched in June as a part of a study of seasonal variations in electron density.

Figure 4.4 shows the electron density profile for rocket flight 14.146 computed by the various radio propagation methods, superimposed upon the electron current measured by the dc probe. The densities derived from differential absorption agree with those of Faraday rotation, thus confirming the collision frequency model. Between 110 and 140 km the standing wave electron density deviates from the electron current, and in this interval, using the mean value of electron density, an aspect correction has been evaluated for the probe current. Below 80 km, the electron density range shows that the electron current indicates an electron density about 10 larger than its actual value. It may also be observed from the two profiles that the electron current possesses good height resolution, whereas the radio propagation data yields only an average electron density over a 1 km interval. Therefore these two measurements may be combined to produce a final electron density profile which possesses the accuracy of the radio propagation technique and the good height resolution of the probe current. For this purpose the ratio of electron density to electron current is computed at every altitude.

It has been shown that the radio propagation data yield an average electron density value centered in the middle of a 1 km interval, whereas the electron current data are read each 0.1 sec, corresponding to 10 electron current values per km. In order to compute the ratio of electron density to electron current at every km, a weighted average

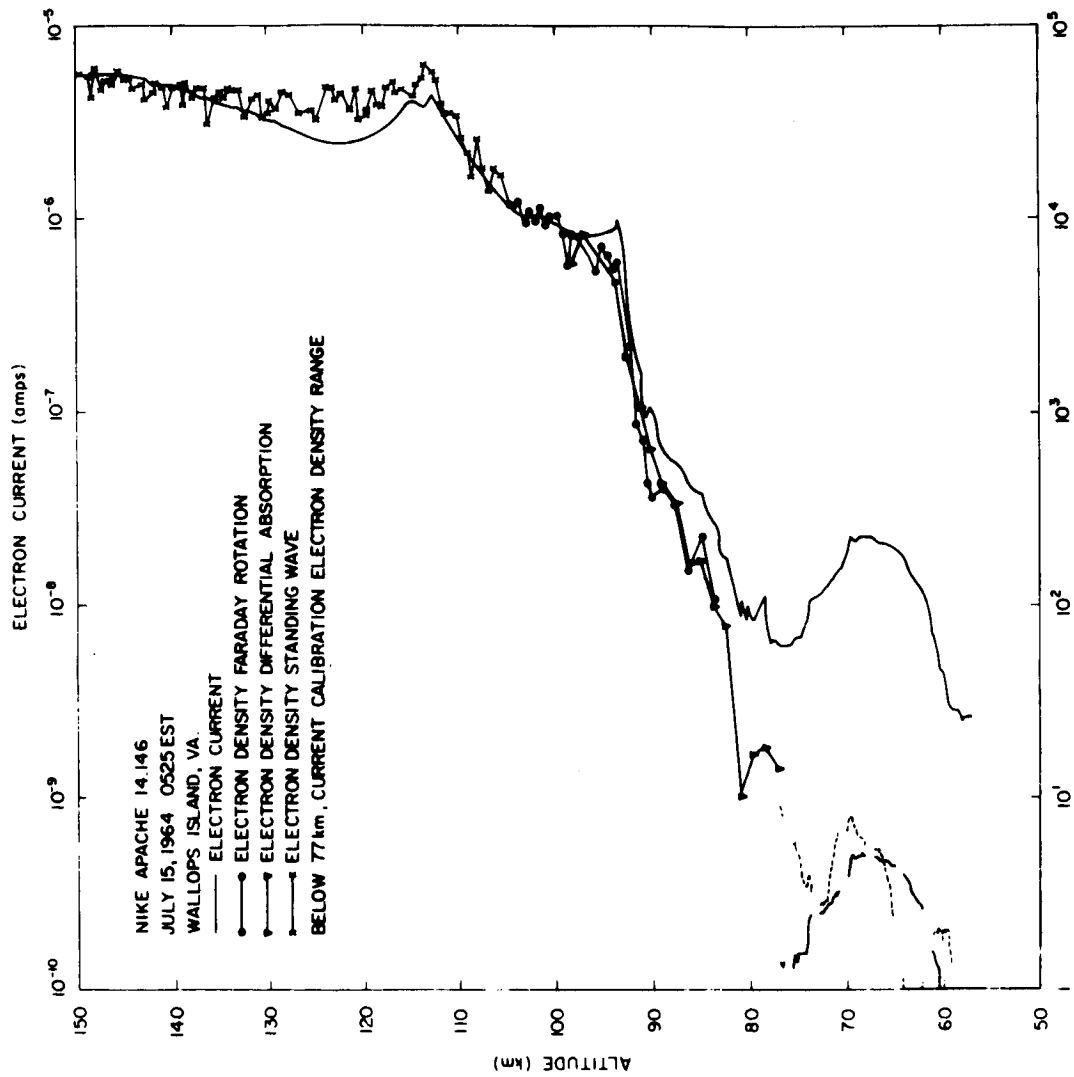

Figure 4.4 Electron density and electron current profiles for rocket flight 14.146.

value of the electron current must be calculated for every 1 km interval. For this purpose, the current reading corresponding to the center of the interval is multiplied by a certain factor, such as 10, the two readings before and after the center value are multiplied by a factor of 9, and so on in decreasing order. The sum of these products is then divided by the sum of the weighting factors, and thus a weighted average is obtained at the center of the interval. The ratio of the average electron density to the weighted average electron current may then be calculated and plotted versus altitude. A smoothed curve is drawn through the various points. When this calibration curve is multiplied by the electron current data, a final electron density profile is obtained. A typical example of the calibration curve is shown in Figure 4.5, and final profiles for 14.144, 14.145, and 14.146 are shown in Figure 4.6.

In Figure 4.6, the electron density in the E-region is seen to increase from its nighttime value to its normal daytime value. At about 70 km, the formation of a C-layer is observed on these flights, as the region is slowly exposed to solar ultraviolet radiation in the wavelength range 1800 to 2900 A^{o}. The C-layer is fully developed in 14.146. Based upon this, it was indicated by Bowhill and Smith (1965) that no photodetachment occurs until radiation at wavelengths smaller than 2900 A^{o} illuminates the region. This lead to the conclusion that O_2^- is not the dominant negative ion in that region at twilight, as had been generally assumed. If O_2^- had been dominant, electrons would have been relased by solar visible radiation and would have been observed on the second flight.

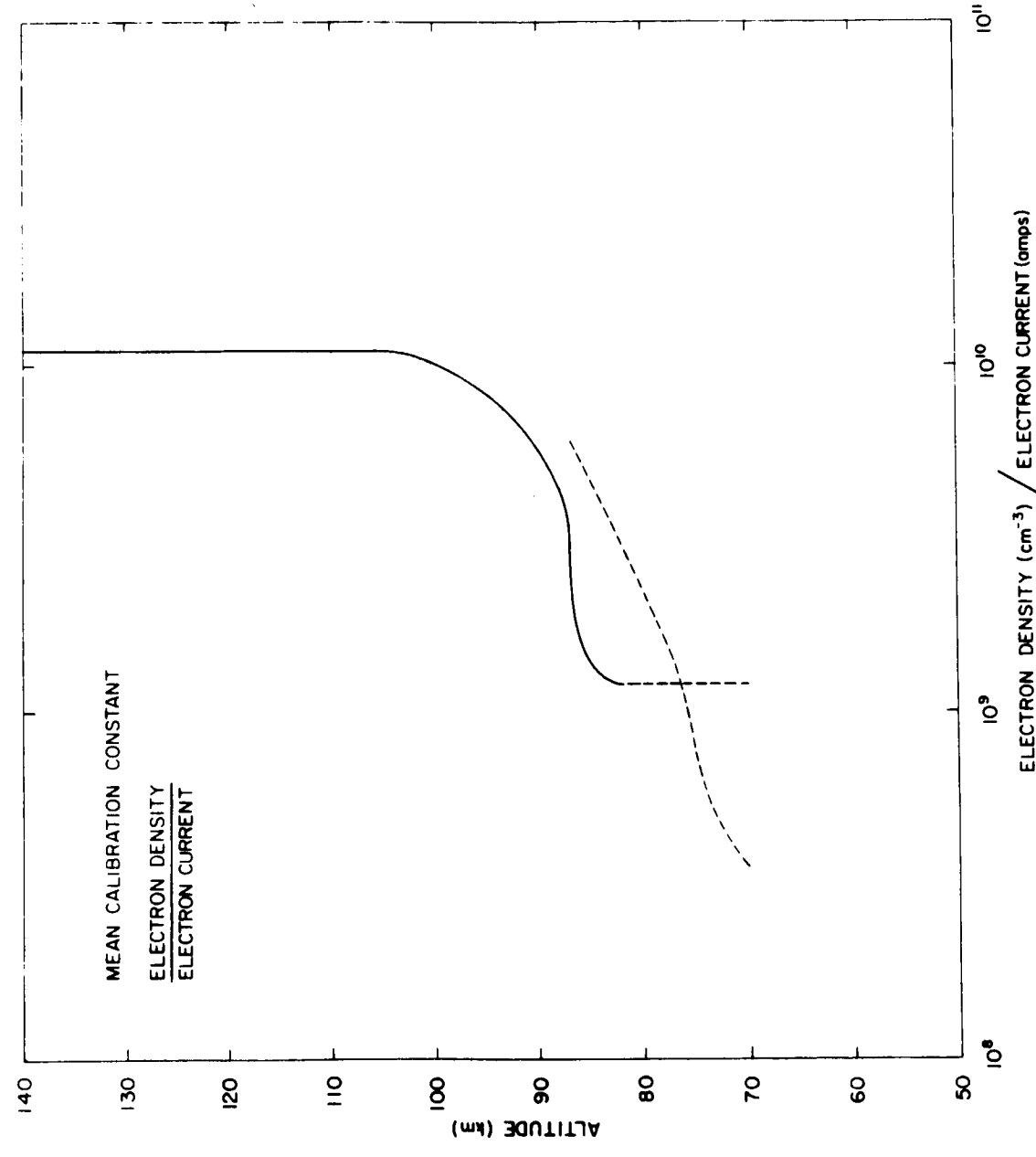

Figure 4.5 Ratio of electron density to electron current versus altitude.

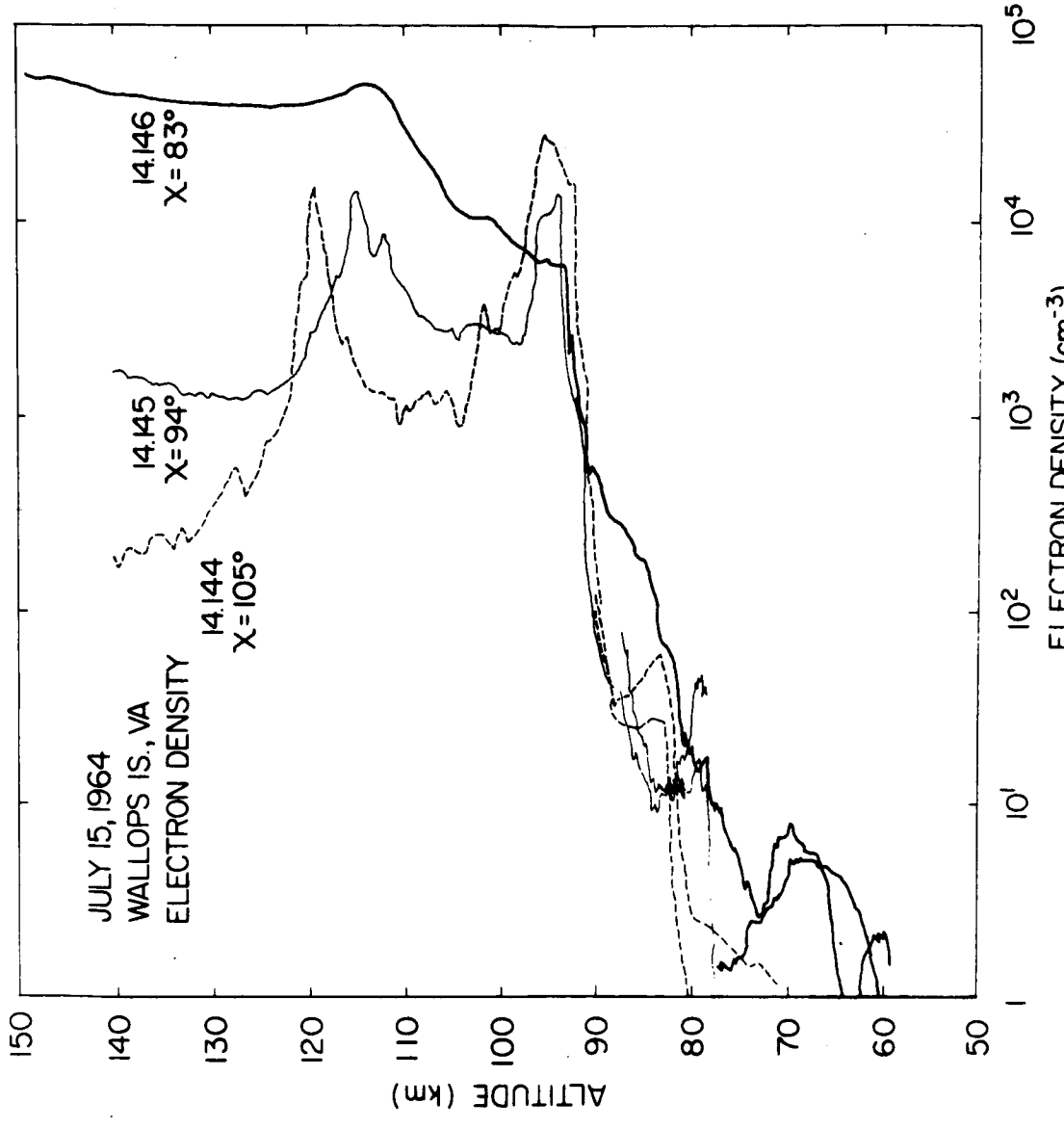

Figure 4.6 Electron density profiles for July 15, 1964 sunrise series.

In addition, two strong Sporadic E layers are observed during each of the three flights, with densities of the order of 10^4 cm^{-3}. The characteristics of these layers have been discussed by Bowhill (1966).

In Figure 4.7, the radio propagation results for the latitude series 14.230, 14.231, and 14.232 are shown. Above 100 km, a constant electron density is observed for all three flights, whereas below 80 km the electron density appears to be largest for the flight closest to the equator and smallest for the southernmost flights.

Finally, a comparison of the monoenergetic collision frequencies for these flights is given in Figure 4.8. Good agreement is observed with the summer and winter results given by Deeks (1966), and the models given by Belrose (1964) and Fejer (1962).

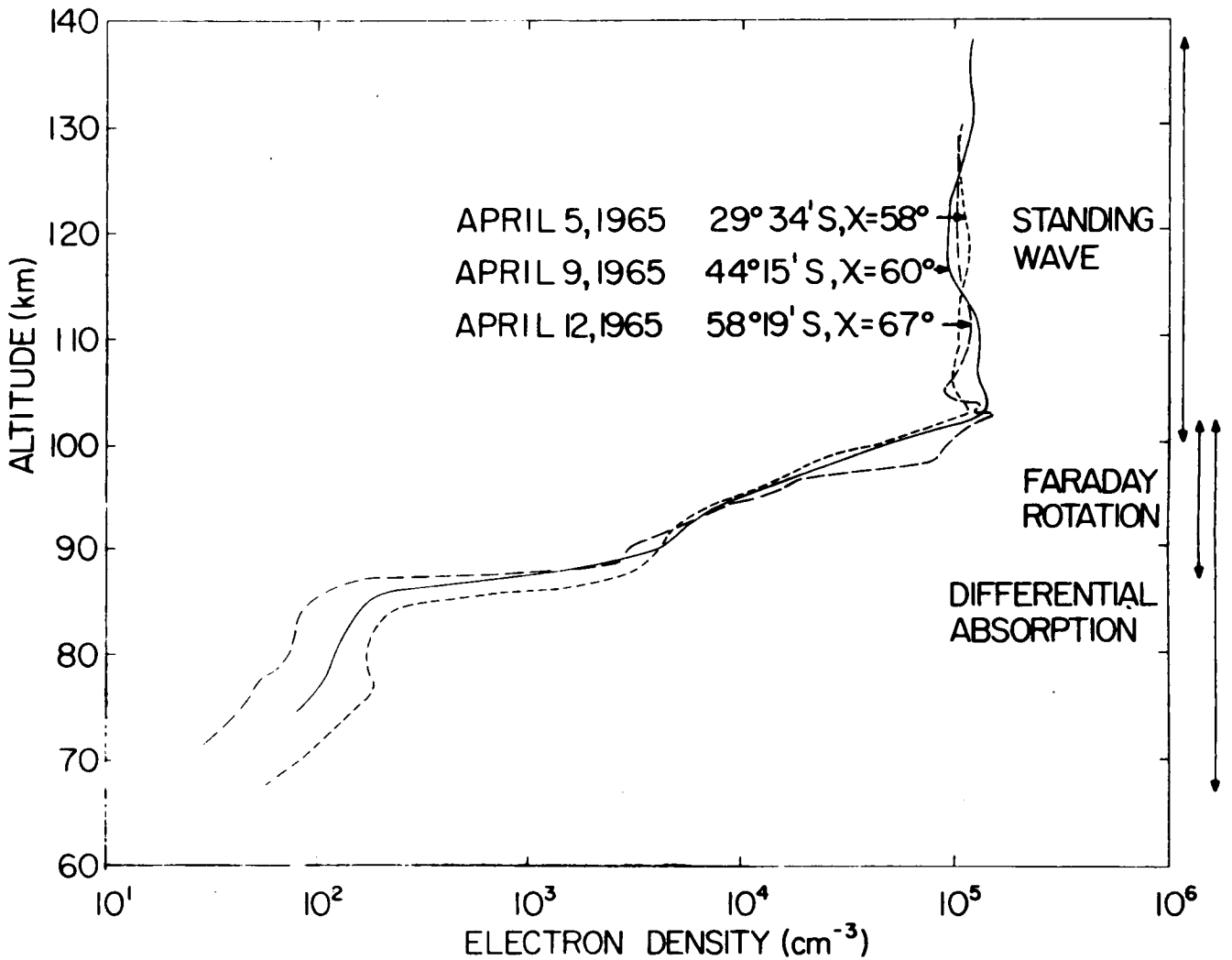

Figure 4.7 Electron density profiles for mobile launch latitude series.

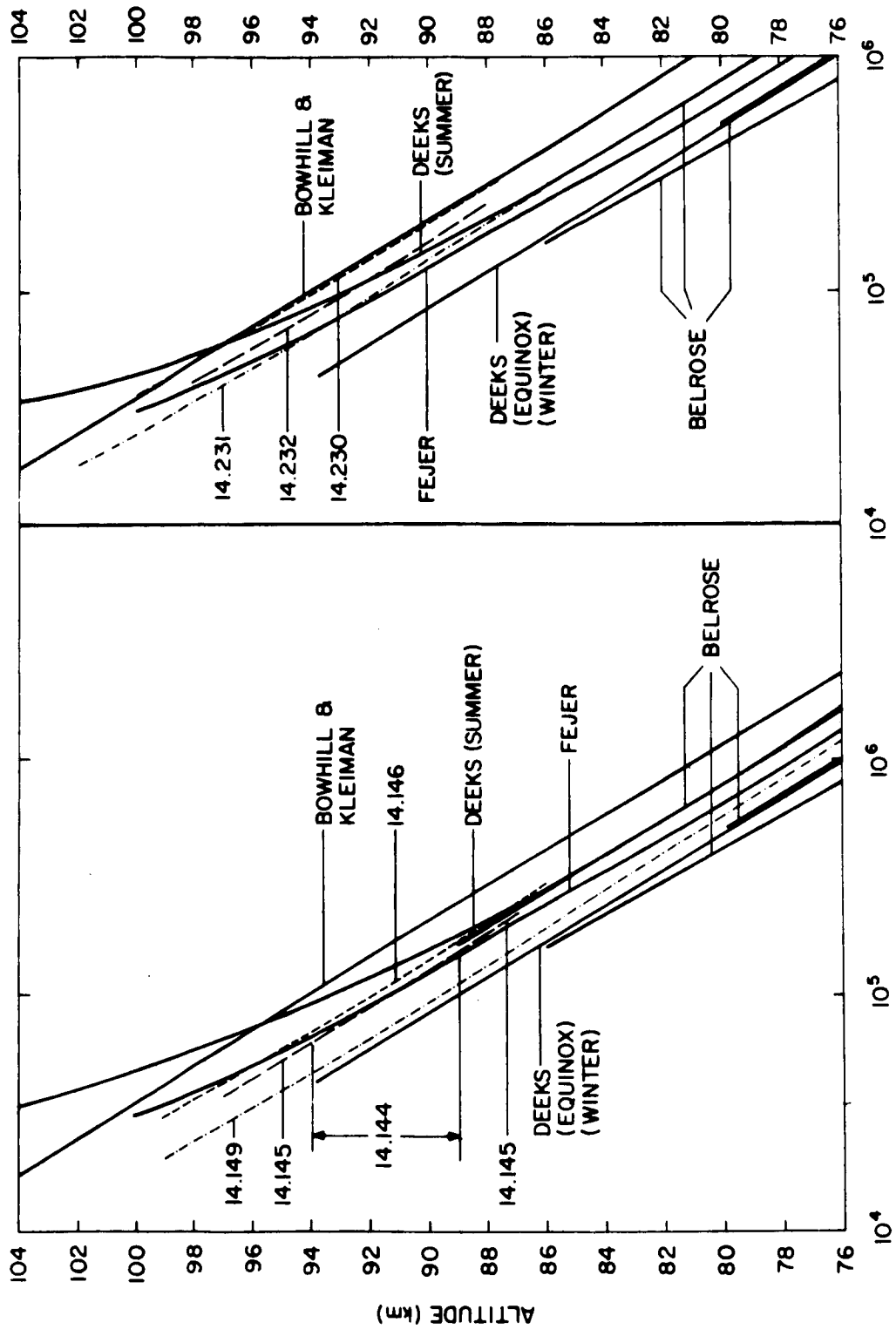

Figure 4.8 Comparison of measured electron collision frequencies.

5. CALCULATION OF ATMOSPHERIC PRESSURE FROM ULTRAVIOLET EXTINCTION MEASUREMENTS

In order to calculate the collision frequency, it is necessary to know the variation of atmospheric pressure with height, since ν was found to be directly proportional to P. For the purpose of the electron density analysis, model atmosphere pressure values have been used. However, it is possible to calculate the atmospheric pressure from the knowledge of the absorption of solar radiation, such as Lyman-α flux. The exact calculation of the observed pressure is valuable for application to the extraction of electron temperatures from collision frequencies as will be described in the next chapter. The method of analysis of ultraviolet radiation measurements and their reduction to atmospheric pressure are discussed in this chapter. Sample results are also given and compared to model atmosphere values.

5.1 Determination of Molecular Oxygen Concentration from Lyman-α Absorption

An accurate determination of the concentration of atmospheric constituents may be obtained from the measurement of absorption of solar radiation in a specific wavelength band. To achieve this purpose, an ion chamber with a particular gas fill and window material may be used. The gas fill provides the desired long wavelength cut-off whereas the window material limits the short wavelength cut-off, thus fixing the bandpass of the radiation measurements (Friedman, 1960).

Throughout much of the vacuum ultraviolet spectrum above 1000 A^{o}, molecular oxygen is the primary absorbing constituent in the upper atmosphere.

Measurement of the absorption of solar hydrogen Lyman-α (1216 Å) may then be used to determine the concentration of molecular oxygen. The height range of these measurements depends on the solar zenith angle because of the change in radiation path, and on the absorbing characteristics of the atmosphere at this wavelength.

For Lyman-α absorption measurements, an ion chamber filled with nitric oxide at a pressure of 20 mm and a 2 mm thick lithium fluoride window has been used (Chubb, et al., 1957). This provides a bandpass of 1050 A^{o} to 1350 A^{o}. In this part of the solar spectrum, Lyman-α is the strongest emission line and its intensity has been estimated to be about 5.1 ergs cm^{-2} sec (Hall, et al., 1963). Thus despite the wide bandpass of the ion chamber, the measured flux can be considered to be essentially all Lyman-α radiation. Figure 5.1 shows the unit optical depth, defined as the altitude at which the intensity of solar radiation drops to 1/e of its value outside the earth's atmosphere, for vertical incidence (Nawrocki, et al., 1961). Lyman-α reaches unit optical depth at about 75 km.

The flux of radiation measured at a certain altitude z is given by the following expression:

$$I(z) = I_{\infty} \exp(-\sigma n_T), \qquad (5.1)$$

where I_{∞} is the flux at the top of the atmosphere, σ is the absorption cross-section at the radiation wavelength and n_T is the columnar number density between the observation point and the sun. For monochromatic

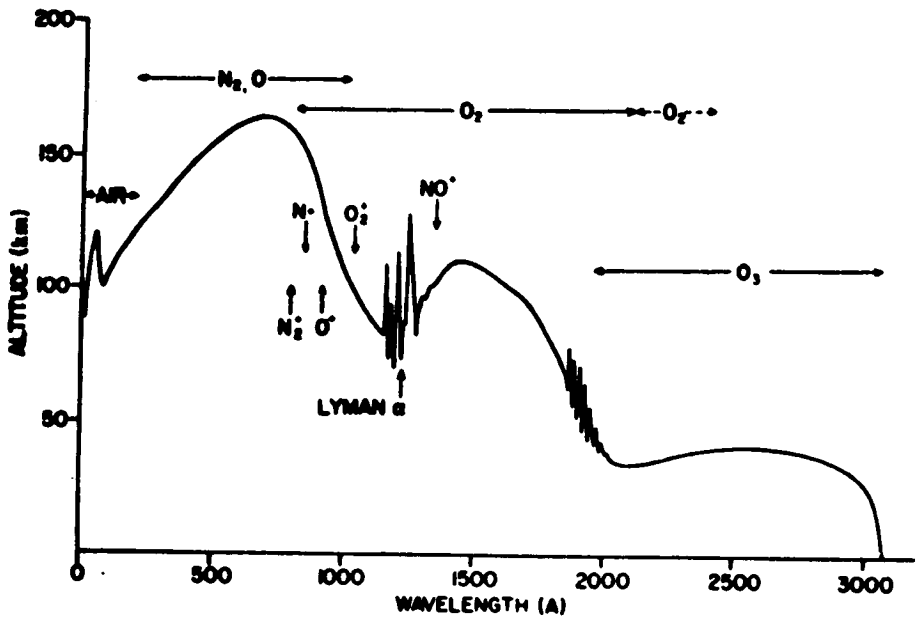

Figure 5.1 Unit optical depth versus wavelength (after Nawrocki, Watanabe, and Smith, 1961).

radiation incident on the chamber, the radiation flux is proportional to the measured ion chamber current.

Equation (5.1) may be written in its differential form:

$$\frac{1}{I}\frac{dI}{dz} = -\sigma\frac{dn_T}{dz}, \tag{5.2}$$

where it is seen that an absolute calibration of the ion chamber to determine I_∞ is not necessary.

The columnar number density may be evaluated for two different approximations. When the solar zenith angle χ is small, the flat earth approximation is valid. Then, from Figure 5.2,

$$\frac{dn_T}{dz} = -n(z)\sec\chi . \tag{5.3}$$

Substituting in Equation (5.2),

$$n(z) = \frac{1}{\sigma\sec\chi}\frac{1}{I}\frac{dI}{dz} . \tag{5.4}$$

This approximation is valid for $\chi \leq 73^\circ$ with a maximum error of 1% which reaches 10% at $\chi = 85^\circ$.

For larger solar zenith angles earth curvature has to be taken into account and approximate solutions may be obtained for $\chi > \frac{\pi}{2}$ and $\chi < \frac{\pi}{2}$. In Equation (5.4) sec χ is replaced by F, the optical depth factor.

Near grazing incidence, $80^\circ < \chi < 90^\circ$, the optical depth factor is the Chapman function Ch (X,χ), where $X = \frac{R+z}{H}$, for a constant scale height

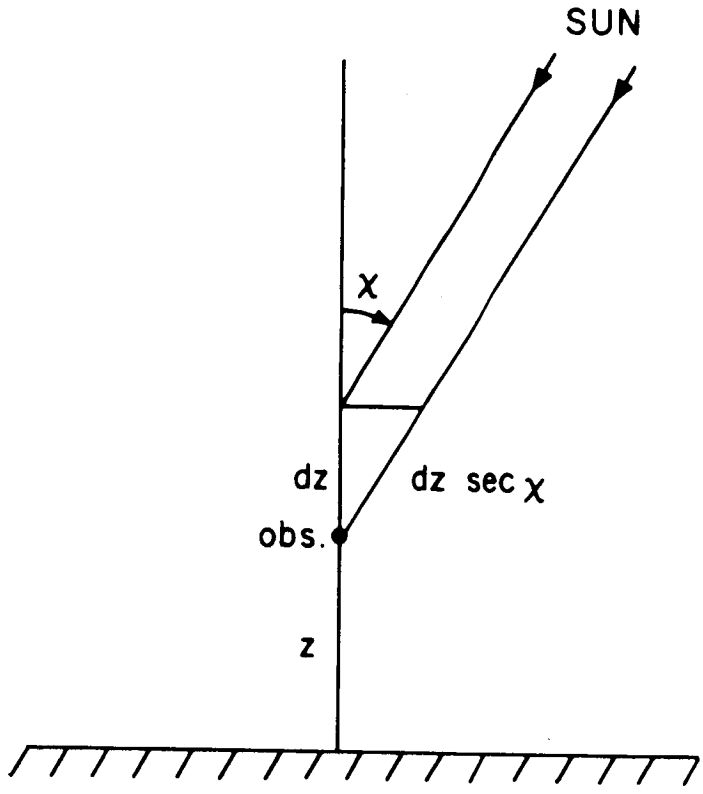

Figure 5.2 Geometry of incoming radiation for flat earth approximation.

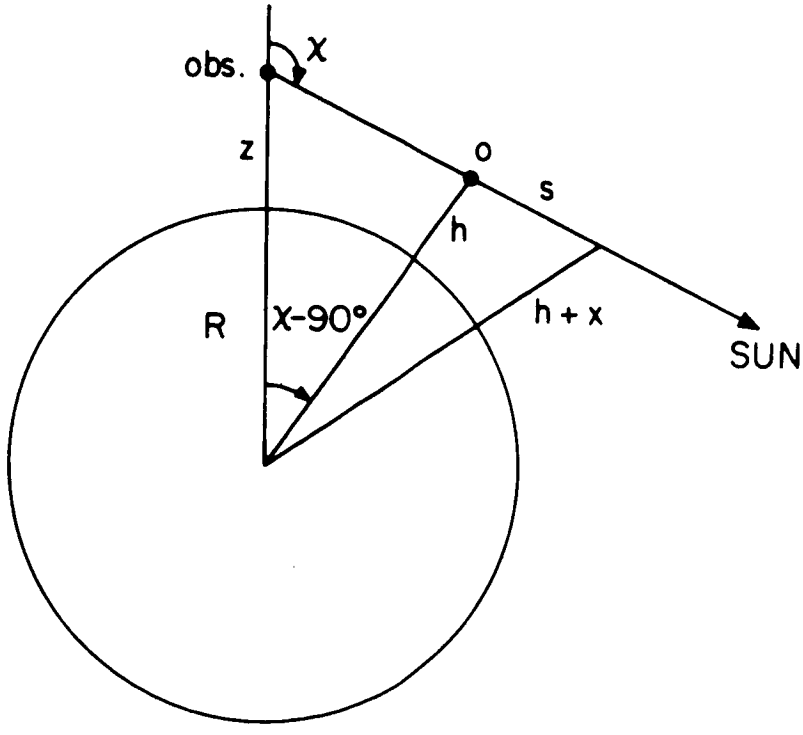

Figure 5.3 Geometry of incoming radiation for general case $\chi > \frac{\pi}{2}$.

gradient. Approximate solutions for different scale heights also have been obtained by Swider (1964).

For $\chi > \frac{\pi}{2}$, the concentration of molecular oxygen is calculated in terms of the minimum ray height, which is the altitude of the closest approach of the radiation to the earth. From the geometry of Figure 5.3, the minimum ray height h is given by the following equation:

$$h=(R + z) \cos (\chi-90^{o}) -R \quad , \tag{5.5}$$

where R is the radius of the earth.

The columnar number density is then given by:

$$n_T(h) = \int_o^{\infty} n \, ds + \int_o^{obs} nds \quad , \tag{5.6}$$

where s is measured away from 0.

Assuming an exponential distribution of density, defined by a constant scale height H, the concentration may be expressed in terms of the minimum ray height as:

$$n(h) = \frac{1}{\sigma F} \frac{1}{I} \frac{dI}{dh} \quad , \tag{5.7}$$

where

$$F \simeq \frac{101.4}{H^{\frac{1}{2}}} \left[1 + \text{erf} \frac{(\chi -90^{o})}{H^{\frac{1}{2}}} \right] . \tag{5.8}$$

Figure 5.4 shows the ion chamber current obtained for the two flights launched at sunrise on July 15, 1964 (Smith and Weeks, 1965). The data

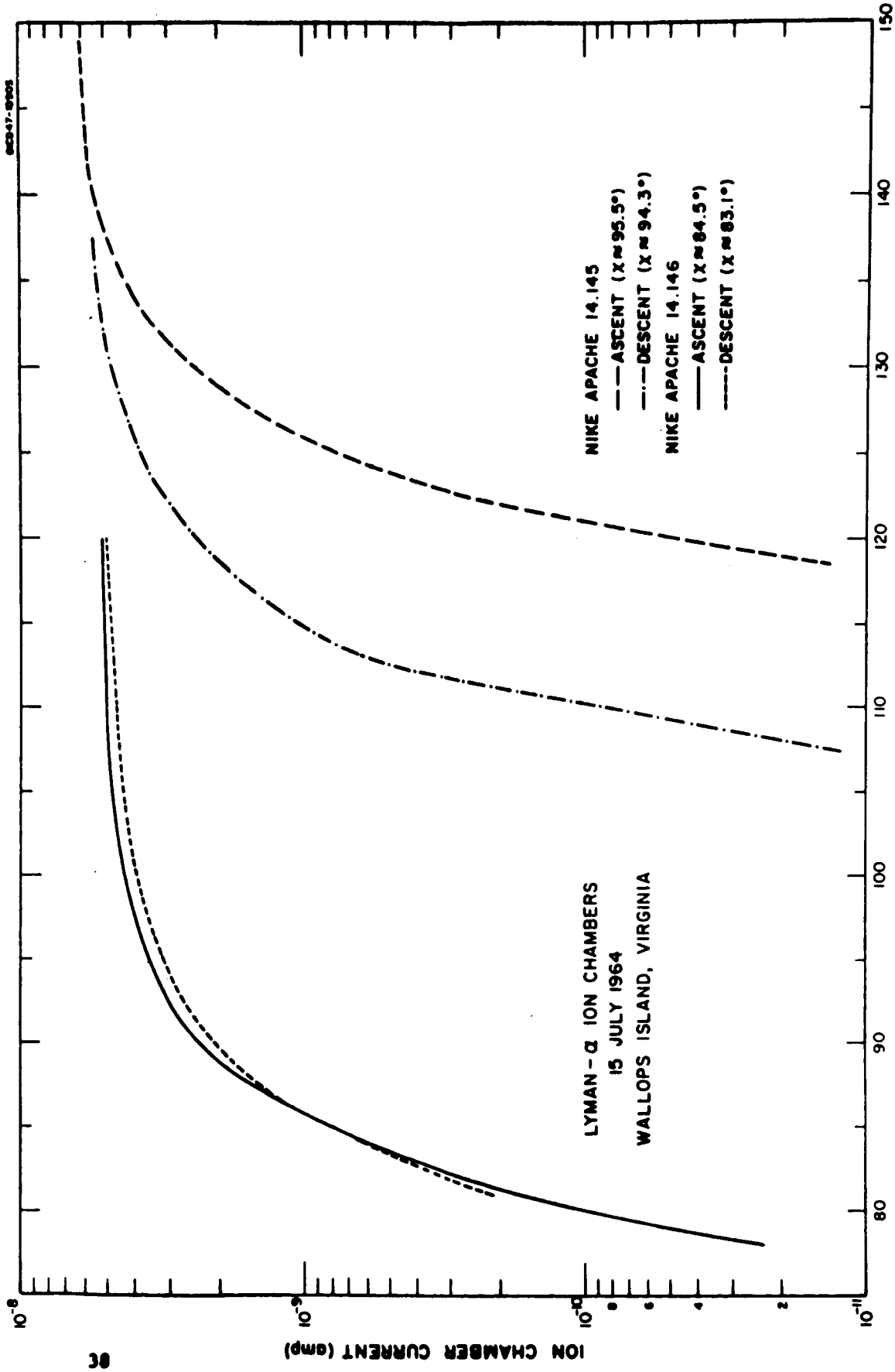

Figure 5.4 Typical Lyman-α ion chamber current profiles (after Smith and Weeks, 1965).

has been normalized to zero aspect angle to account for the direction of the incoming radiation. It is observed that a small difference of zenith angle between ascent and descent data produces a pronounced effect on the shape and range of the absorption profiles.

In the derivation of molecular oxygen concentration from this data, a value of .27 cm^{-1} has been used for the absorption coefficient, α, of molecular oxygen at Lyman-α wavelength (Watanabe, 1958). This is related to the absorption cross-section by

$$\sigma = \frac{\alpha}{N} \quad , \tag{5.9}$$

where N is the number density of molecules per unit volume at normal temperature and pressure (2.69×10^{19} cm^{-3}). The cross section used is thus 1×10^{-20} cm^2.

Typical molecular oxygen density profiles are shown in Figure 5.5 (Smith and Weeks, 1965). These results are in very good agreement with molecular oxygen concentration given in most atmospheric models.

The effect of zenith angle on the altitude range of measurements is quite noticeable. At $\chi=84^{o}$ the range is about 80 to 108 km, whereas at $\chi=95^{o}$ the range is about 90 to 112 km.

These plotted data fit well the average scale height of 6.6 km. The difference in number density between the two flights may be due to the approximations applied for the calculation of 14.145 where $\chi > \frac{\pi}{2}$.

The technique to measure the Lyman-α radiation flux is relatively simple and quite dependable. The main uncertainty in these measurements may develop from the absorption coefficient where errors as large as 25% may be introduced (Smith and Weeks, 1965).

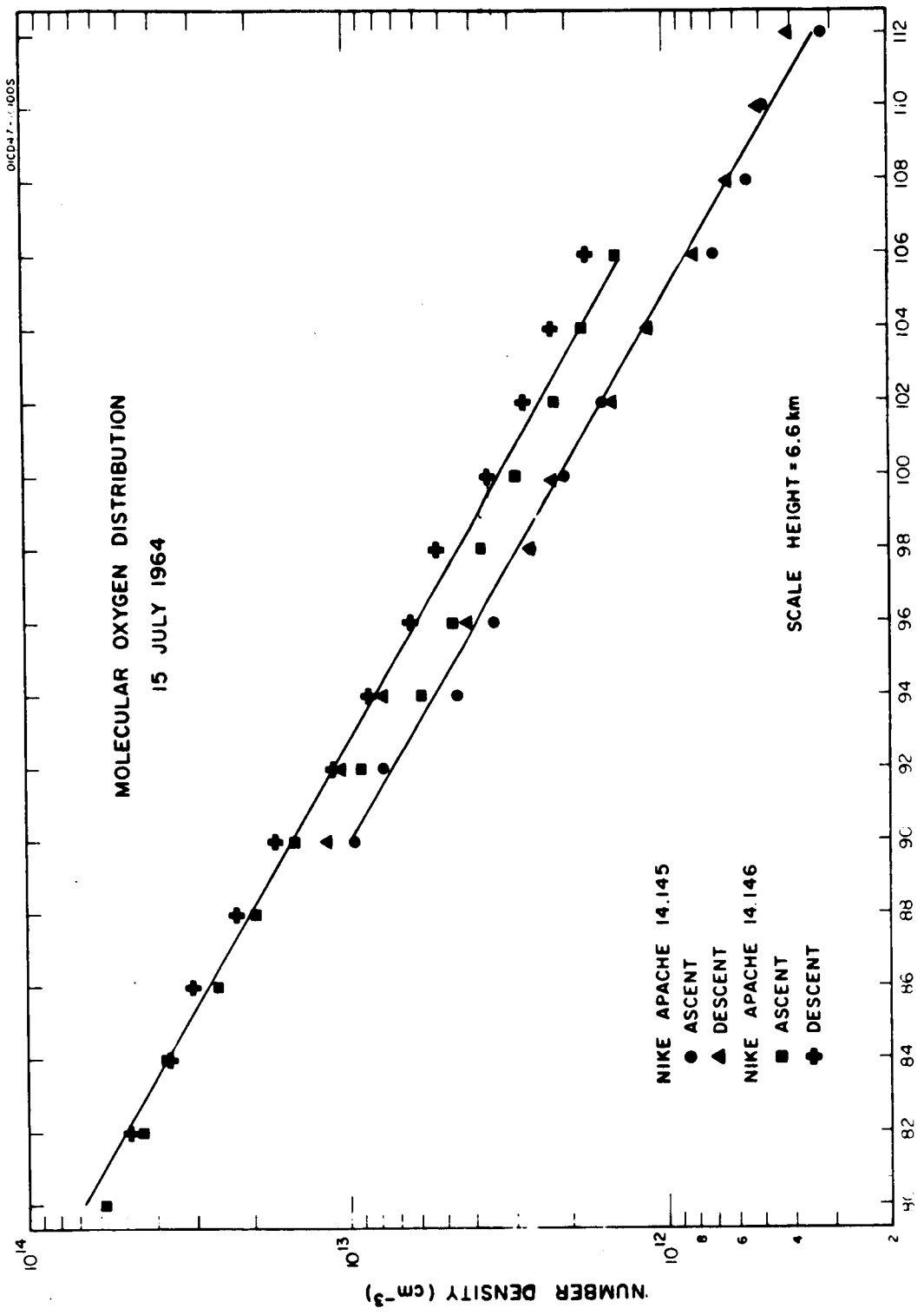

Figure 5.5 Typical molecular oxygen density profiles (after Smith and Weeks, 1965).

5.2. Calculation Of Atmospheric Pressure From Ultraviolet Extinction Measurement.

In the preceeding section it has been shown that the molecular oxygen concentration may be obtained from the measurement of Lyman-α absorption. The general equation governing this measurement may be expressed as

$$n(O_2) = \frac{1}{\sigma F} J \quad , \tag{5.10}$$

where

$$J = \frac{1}{I} \frac{dI}{dz} \quad \text{for } \chi < \frac{\pi}{2} \quad , \tag{5.11}$$

or

$$J = \frac{1}{I} \frac{dI}{dh} \quad \text{for } \chi > \frac{\pi}{2} \quad . \tag{5.12}$$

Solving for J in Equation (5.10) and integrating from z to infinity, we obtain

$$\int_z^\infty J dz = \sigma \int_z^\infty F\, n(O_2)\, dz \quad . \tag{5.13}$$

The optical depth factor F is a function of zenith angle χ and scale height, H. However, since this analysis is concerned with a relatively small altitude range, mainly 80 to 100 km, in which an average scale height is dominant, and across which the zenith angle barely changes, F may be considered independent of altitude. In the following numerical analysis, the optical depth factor is calculated at one scale height above

the lower altitude limit, since only an average value of F can be assumed across the integration interval. In this manner, F may be assumed constant and the integration is simplified. The value one scale height was determined by carrying out the integration with a linear function being assumed for the optical depth factor.

In Equation (5.4), the concentration of molecular oxygen has already been determined. Then, a model atmosphere may be used to obtain the nitrogen and atomic oxygen concentrations and therefore determine the $\frac{n(O_2)}{n(M)}$ ratio. For this purpose a model atmosphere suggested by Colegrove, Hanson and Johnson (1965) has been used, for which the ratio $\frac{n(O)}{n(O_2)}$ at 120 km is taken as unity, corresponding to an eddy diffusion coefficient of 4.04×10^6 cm^2 sec^{-1} which agrees with experimentally estimated values. Figure 5.6 shows this atmospheric model together with the measured molecular oxygen concentration for the two flights mentioned earlier.

In the evaluation of the ratio of molecular oxygen concentration to the total number density, dissociation of molecular oxygen at the higher altitudes must be taken into account. However, the dissociation of molecular oxygen, which is an important chemical effect of solar radiation at ultraviolet wavelengths, takes place principally around the 110 km level. Therefore, below 100 km, the ratio of molecular oxygen to the total number density may be assumed constant.

Based upon the above, a new average constant, K_r, may be defined as

$$K_r = \frac{n(O_2)}{n(M)} \quad , \tag{5.14}$$

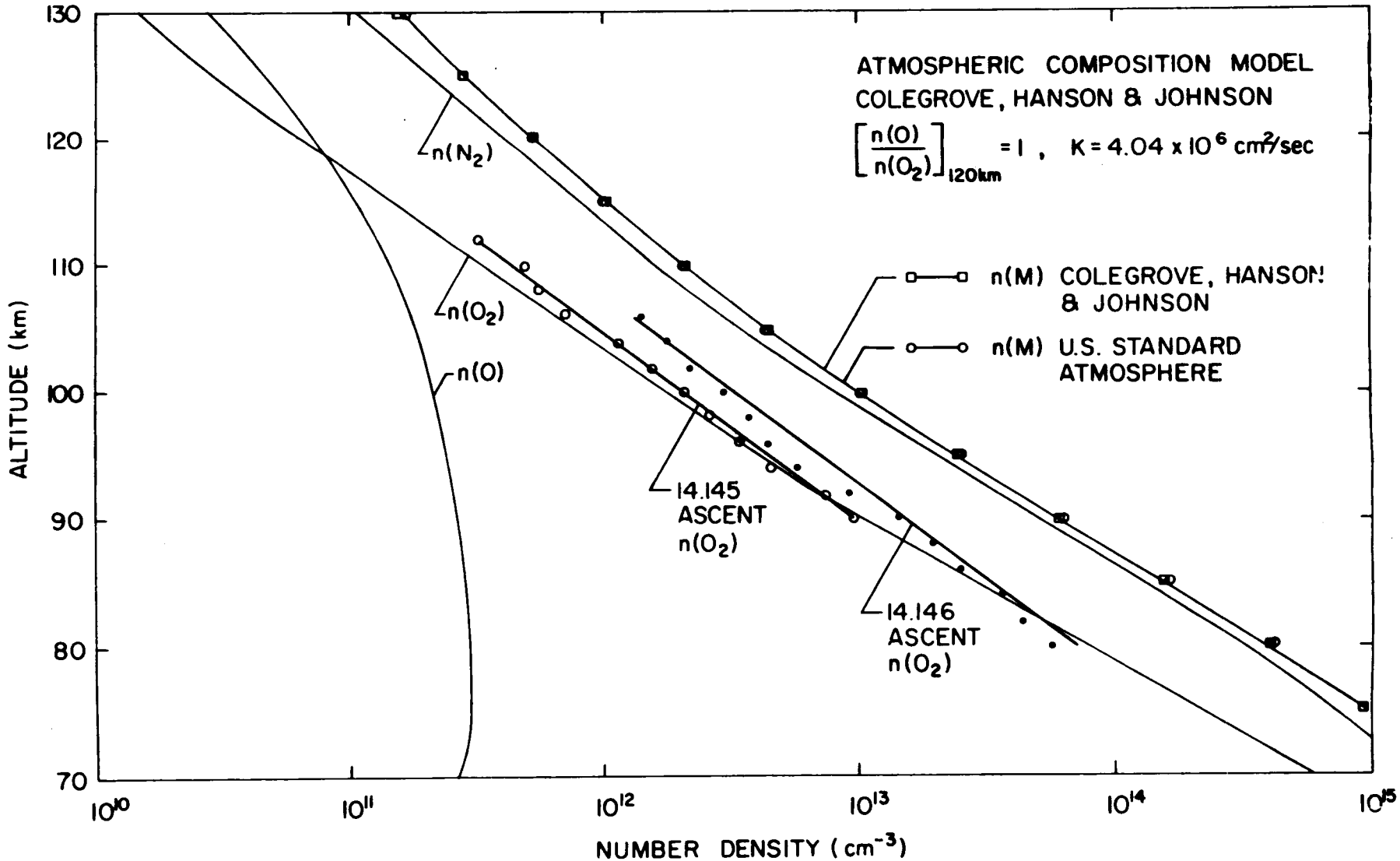

Figure 5.6 Concentration of the atmospheric constituents versus altitude (after Colegrove, Hanson and Johnson, 1965).

Equation (5.13) may then be expressed as

$$\int_z^\infty J dz = \sigma' F K_r \int_z^\infty n(M) dz \, . \tag{5.15}$$

The total number density is related to the atmospheric pressure by the perfect gas equation

$$P(M) = n(M)\, kT \, , \tag{5.16}$$

where k is Boltzmann's constant, and T the absolute temperature. The use of this equation in the D-and lower E-regions is justified by the very low pressures existing in these regions.

Furthermore, from the consideration of the hydrostatic equation

$$\frac{dP}{dz} = \frac{-P}{H} \, , \tag{5.17}$$

an exponential atmosphere may be assumed if H is considered constant in the region of interest, mainly 80 to 100 km. In this region, the constituents of the earth's atmosphere are in a well mixed state, thus giving a uniform composition. The temperature gradient is small in that region and justifies the assumption of an isothermal model. Finally, neglecting the variation of gravity in that small range, the pressure distribution may be expressed as

$$P(M) = P_o(M) \exp\left(- \frac{z - z_o}{H} \right) \tag{5.18}$$

where the subscript o refers to a reference height $z=z_o$.

Equation (5.15) may therefore be evaluated in terms of pressure

$$\int_z^\infty Jdz = \sigma FK_r \int_z^\infty \frac{P(M)}{kT_n}\, dz$$

$$= \frac{\sigma FK_r}{kT_n} \int_z^\infty P_o(M) \exp\left(-\frac{z-z_o}{H}\right) dz$$

$$= \frac{\sigma FK_r P(M)}{kT_n} \qquad (5.19)$$

and the observed pressure is then written as

$$P(M) = \frac{kT_n \int_z^\infty Jdz}{\sigma FK_r H} \qquad (5.20)$$

Table 5.1 shows the results of the computations for 14.145 and 14.146. This is compared with atmospheric pressure given by the U.S. Standard Atmosphere, 1962. For 14.145, the observed pressure is seen to differ from model atmosphere values by an average factor of 1.1, while for 14.146 the factor is 0.98. Despite the several approximations made throughout the analysis, particularly in the optical depth evaluation, this analytical method seems to yield favorable results.

Altitude (km)	14.145	U.S. Standard Atmosphere 1962	14.146
80		10.35	8.37
82		7.18	7.08
84		4.97	5.83
86		3.43	3.31
88		2.37	2.49
90	1.42	1.64	1.91
92	1.14	1.14	1.49
94	.803	.806	1.11
96	.565	.575	.69
98	.408	.413	.572
100	.36	.3	.421

Table 5.1. Comparison of computed atmospheric pressure (dynes/cm^2) with U.S. Standard Atmosphere 1962.

6. CALCULATION OF ELECTRON TEMPERATURE FROM ABSORPTION MEASUREMENTS

The following sections describe the conflicting theories pertaining to the thermal equilibrium of electrons in the lower ionosphere, and the laboratory measurements of the collision frequency in air, upon which the electron temperature calculations are based. A mathematical formula is developed for the electron temperature, and applied to the data from five rocket experiments. The electron temperature is then compared with the neutral temperature, which is extracted from the scale height of the molecular oxygen, and the results are discussed.

6.1 Theories Relating Electron and Neutral Temperatures in the D-Region

In recent years, it has become evident that the electron temperature, T_e, exceeds the neutral temperature, T_n, in the upper atmospheric regions, mainly above 150 km (Evans and Lowenthal, 1964; Brace, et al., 1965).

In the D-region, however, it has been customary to assume that the electrons have a Maxwellian velocity distribution characterized by T_e, under thermal equilibrium conditions. This important question of thermal equilibrium of electrons with neutral molecules has led to several conflicting theories.

From a study of the competing processes of collisional energy loss and electron dissociative attachment to oxygen molecules, Sears (1963) has shown that a knowledge of the characteristic times of these processes may be used to relate temperature and electron density measurements. The energy distribution for the photodetachment of electrons from negative

ions, as obtained from experimental data, was found to have an average energy of 2.9 ev. This non-thermal energy leads him to conclude that T_e would exceed T_n in the D-region, and to support the cross modulation observations made by Rumi (1962) who has measured an electron temperature of 1200°K at an altitude of 40 km. In addition, Belrose and Hewitt (1964) have shown that the electron collision frequency in the D-region is strongly correlated with solar activity. They suggest that since electron collision frequency depends on electron temperature, the results of this correlation tend to indicate that T_e might be higher than T_n, under quiet conditions.

On the other hand, a recent study of the effects of elastic collisions and rotational and vibrational excitation of molecules on the dissipation of electron energy, has led Dalgarno and Henry (1965) to make detailed estimates of the rates of energy loss of electrons in the D-region. Their calculations show that the electron gas has a negligible non-thermal component and that the main mechanism tending to establish thermal equilibrium consists of rotational transitions in molecular nitrogen. Therefore if electrons in the D-region have a Maxwellian distribution, it will be characterized by T_n.

In the upper atmospheric regions above 150 km, it is found that energy loss through elastic collisions with ambient electrons is an important mechanism for heating the latter and maintaining T_e above T_n (Dalgarno, et al. 1963). In the D-region, on the contrary, energy loss in elastic collisions with molecules in negligible compared to loss through rotational transitions.

It is the object of this section to demonstrate how an average value of electron temperature may be calculated from radio absorption measurements in the D-region for several experiments conducted at various solar zenith angles. The results, it will be observed, support the Dalgarno and Henry theory whereby thermal equilibrium conditions are seen to prevail in the D-region.

6.2 Theory of Calculation of Electron Temperature from Collision Frequency

Several methods of measurement of electron temperatures in the upper atmosphere have been developed, most recent of which is the Langmuir probe technique (Spencer, et al., 1962). From the current-voltage characteristic of the probe, the electron temperature is obtained as a function of altitude. This procedure, however, is not useful for heights below 100 km where the mean free path is not large compared with the Debye length.

In view of the above, a method to obtain electron temperatures from the collision frequency of electrons with neutrals may be considered.

The electron collision frequency, ν, is usually expressed in terms of the following equation

$$\nu = N \sigma v \tag{6.1}$$

where N is the electron gas density, σ is the collision cross-section, and v is the electron velocity.

As mentioned in Section 2.1, the Appleton-Hartree formulas assume that the collision frequency is independent of electron velocity. This

is a special case of possible velocity dependences for the collision frequency, namely ν is constant.

In recent years, however, measurements of collision frequency made in the laboratory for various gases has shown that the velocity dependence of collision frequency varies from gas to gas. For nitrogen, the major constituent of the ionosphere, Phelps and Pack (1959) used an improved version of the electron drift velocity tube (Bradbury and Nielsen, 1936) to measure the mobility of electrons at such low electric fields that the electrons are in thermal equilibrium with the gas. The measurement was in terms of the product of the electron mobility and the gas density at 77^{o} K and at room temperatures. These results were then expressed in terms of the momentum transfer collision frequencies for monoenergetic electrons ($u = kT$) as a function of electron energy. These data are presented in Figure 6.1, where it is shown that the electron collision frequency is very nearly directly proportional to electron energy, or T_e.

This result has been supported by thermal equilibrium measurements of microwave conductivity made by Phelps, Fundingsland, and Brown (1951). The results are also shown in Figure 6.1 and are seen to agree very well with the Phelps and Pack function.

Even though nitrogen is the major constituent of the ionosphere, an estimate of collision frequency of electrons in oxygen must be made before the above results are generalized for air. Drift velocity measurements (Nielsen and Bradbury, 1937) and diffusion data (Healey and Reed, 1951) in oxygen have shown that collision frequency of electrons in

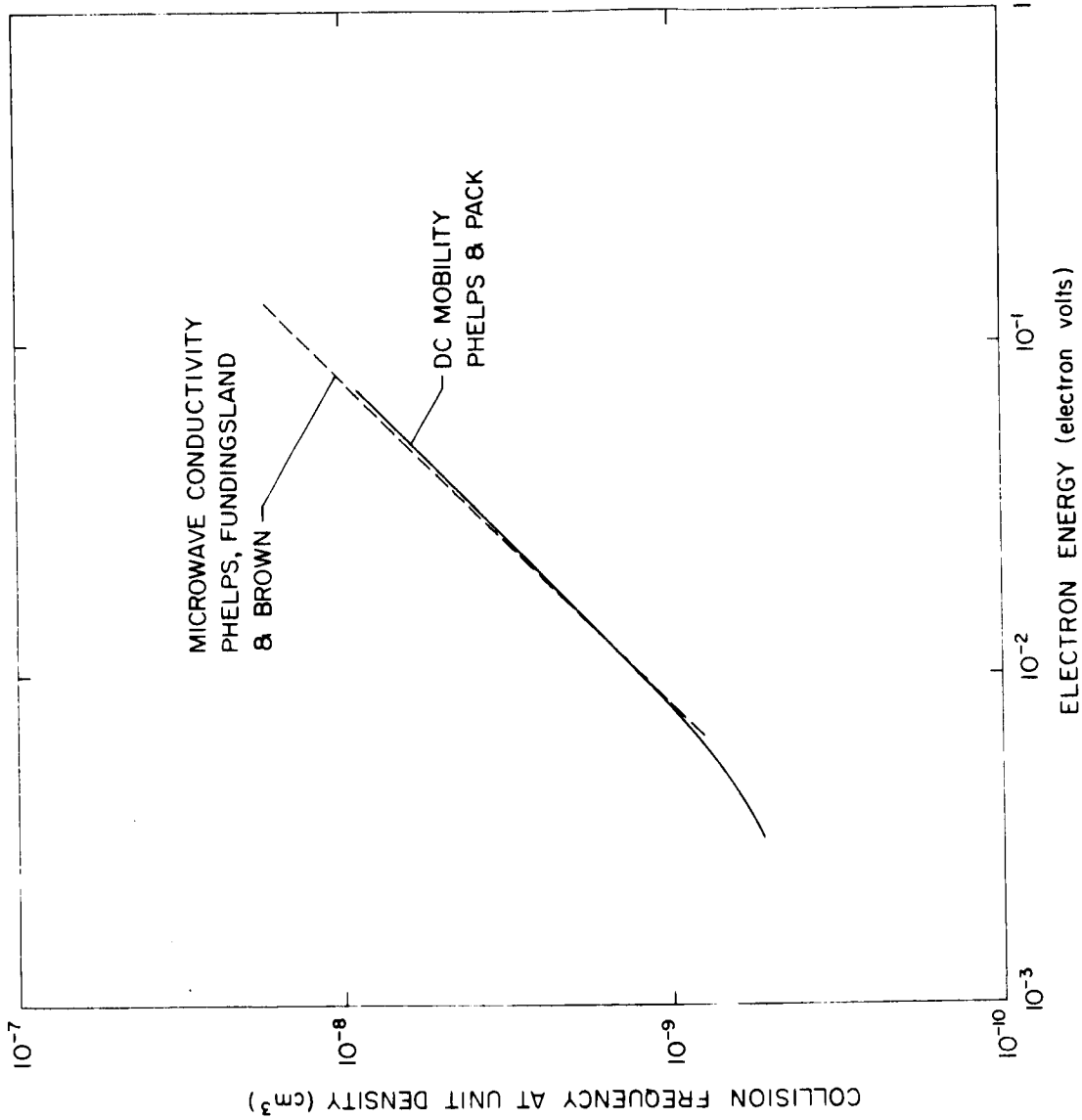

Figure 6.1 Electron collision frequency at unit density versus electron energy (after Phelps and Pack, 1959).

oxygen is about two-thirds of that for nitrogen down to 0.2 electron volts. Assuming that this same ratio holds at thermal energies, the errors introduced when collision frequency for air is taken equal to that for the nitrogen alone is less than 7%. Moreover, Huxley (1959) has compared average collision cross sections obtained from measurements in air and in nitrogen and concluded that the effect of oxygen is negligible.

In air, therefore, the collision frequency is directly proportional to v^2 or to T_e.

Comparison of these and other laboratory measurements (Crompton and Sutton, 1952; Anderson and Goldstein, 1956) with rocket measurements (Kane, 1959) showed a factor of three difference between both results. In an attempt to resolve this discrepancy, Nicolet (1959) analyzed the results in term of collision cross sections. He showed that below the F1-layer electronic collisions are mainly with neutral particles. The collision frequency was then expressed directly proportional to the mean thermal velocity of electrons at T_e as

$$\nu = \frac{4}{3} \pi\sigma^2 \, n \left(\frac{8kT_e}{\pi m_e} \right)^{\frac{1}{2}} , \qquad (6.2)$$

where $\pi\sigma^2$, the cross section was assumed constant. By decreasing the cross section value until the experimental and observational data were reconciled, an expression was written for the collision frequency of electrons with neutral particles and was adapted for aeronomic purposes. The new cross section, namely 15 au, (1.32×10^{-15} cm^2) agrees with that given by Phelps, Fundingsland, and Brown.

In view of the Phelps and Pack results, a generalization of the Appleton-Hartree magneto-ionic formulas has been derived by Sen and Wyller (1960). As stated in Section 2.3, correction factors for ν_{AH} are derived in the asymptotic limits of $\nu \ll \omega$ and $\nu \gg \omega$. This treatment has finally correlated successfully the rocket measurements with the laboratory results.

6.3 Method of Calculation of Electron Temperature

Based upon the Phelps and Pack results, the collision frequency of monoenergetic electrons, ν_m, in air may be expressed as

$$\frac{\nu_m}{n} = K_{pp} E \quad , \tag{6.3}$$

where n is the number density, and E is the most probable electron energy.

Substituting for E and solving for T_e, the following equation is obtained

$$T_e = \left(\frac{e}{k K_{pp}} \right) \frac{\nu_m}{n} \quad . \tag{6.4}$$

In Section 4.2, an Appleton-Hartree collision model has been derived and expressed as

$$\nu_{AH} = k_2 P_m \quad , \tag{6.5}$$

in which ν_{AH} has been assumed independent of electron velocity and where P_m indicates model atmospheric pressure.

By means of the Sen and Wyller approximations, ν_{AH} may now be associated with the energy distribution by multiplying ν_{AH} by the following factors,

$$\nu_m = \frac{2}{5}\nu_{AH} \qquad \text{in the limit} \qquad \nu \ll \omega \pm s$$

$$\nu_m = \frac{2}{3}\nu_{AH} \qquad \text{in the limit} \qquad \nu \gg \omega \pm s \tag{6.6}$$

The radio propagation experiment has been undertaken with frequencies 3.385 mc and 2.225 mc, and in the D-region, around 80 km, the collision frequency is of the order of 10^6 sec^{-1}. Therefore, for altitudes above 80 km, $\nu \ll \omega \pm s$ and the approximation $\nu_m = \frac{2}{5}\nu_{AH}$ may be used.

Substituting $\nu_m = \frac{2}{5}\nu_{AH}$ in Equation (4), we obtain

$$T_e = \left(\frac{2}{5}\ \frac{e}{kK_{pp}}\right)\ \frac{\nu_{AH}}{n} \ . \tag{6.7}$$

By means of the perfect gas law, the number density n may be written in terms of the observed pressure calculated in Section 5.2 as

$$n = \frac{P_{obs}}{kT_n} = \frac{\int_z^\infty J dz}{\sigma F K_r H} \ , \tag{6.8}$$

and the electron temperature is then finally expressed as

$$T_e = \left(\frac{2}{5}\ \frac{e\sigma}{kK_{pp}}\right)\ F\ H\ K_r\ \frac{\nu_{AH}}{\int_z^\infty J dz} \ . \tag{6.9}$$

Since only one measurement of ν from the absorption data is made for each rocket experiment, only an average T_e may be calculated. The range of altitudes in which this average value is valid is governed by the altitude limits at which the collision model is derived, and by the altitude limits of the Lyman-α absorption measurements. A reasonable estimate of this range would be from 80 to 100 km.

In Equation (6.9) the pertinent parameters are calculated in the following manner. An average value of $\frac{\nu_{AH}}{\int J dz}$ is obtained for each experiment in the specific altitude range. From the molecular oxygen concentration, an average value of H is calculated, and a model atmosphere is constructed. The ratio $K_r \left(n(O_2)/n(M)\right)$ is then obtained from that model. As described for the pressure calculation in Section 5.2, the optical depth F is evaluated at one scale height above the lower boundary altitude.

6.4 Calculation of Neutral Temperatures from Molecular Oxygen Scale Height

Since our measurements are concerned with the D-region in which the constituents of the upper atmosphere are in a well mixed state, the scale height governing the distribution of molecular oxygen concentration may be applied to all the constituents. If an average scale height is fitted over the region of interest, an average neutral temperature may be extracted. This follows from the definition of scale height,

$$H = \frac{kT_n}{mMg} , \qquad (6.10)$$

where k is Boltzmann's constant, T_n is the neutral temperature, m is the atomic mass unit, M is the mean molecular mass, and g is the acceleration due to gravity.

Formulas (6.9) and (6.10), used to calculate electron and neutral temperatures, have been applied to several rocket experiments. Description of the conditions of launch and the temperature results will now be presented.

6.5 Observed Difference Between Electron and Neutral Temperatures

In order to evaluate electron and neutral temperatures in the D-region, it is necessary to measure the electron collision frequency and to determine the molecular oxygen concentration in that region. It was shown in Section 4.2 that the electron collision frequency may be extracted from the measurement of the differential absorption of two waves traveling through the ionosphere, and from the knowledge of the electron density obtained from Faraday rotation. The molecular oxygen concentration may be determined from the measurement of the absorption of the Lyman-α radiation by means of ion chambers. Therefore, a payload containing the radio propagation experiment and ultraviolet ion chambers is adequate for the determination of electron and neutral temperatures. Such a payload was designated "Type A" in Section 3.3. Several of the Type A payloads launched as a part of this program, that have yielded molecular oxygen densities, and for which electron collision frequency models have been obtained, are listed in Table 6.1. The rocket flights numbered 14.145 and 14.146 were the second and third of a three-rocket sunrise series, launched at D-region sunrise and after ground sunrise, respectively, on July 15, 1964. The rockets numbered 14.230 and 14.231 were a part of a five-rocket series launched in the southern hemisphere from aboard USNS CROATAN, NASA's mobile carrier,

Flight		14.145	14.146	14.231	14.232	14.246
Date		July 15, 1964	July 15, 1964	April 9, 1965	April 12, 1965	June 17, 1965
Launch Time		0420 EST	0525 EST	1418:15 EST	1214:02 EST	1641 EST
Latitude		38^{o}N	38^{o}N	44^{o}15'S	58^{o}19'S	38^{o}N
Zenith Angle		96^{o}	85^{o}	60^{o}	67^{o}	60^{o}
Collision Model [ν_{AH}=kP ; P:mm Hg]		$k=2.5 \times 10^{8}$	$k=2.90 \times 10^{8}$	$k=2.69 \times 10^{8}$	$k=3.29 \times 10^{8}$	$k=3.03 \times 10^{8}$
Scale Height		6.1 km	6.6 km	6.2 km	8.6 km	5.9 km
Measurement Altitude Range		90-98 km	80-100 km	86-92 km	88-98 km	80-96 km
Electron Temperature		199^{o}K	222^{o}K	223^{o}K	284^{o}K	203^{o}K
Neutral Temperature		201^{o}K	218^{o}K	206^{o}K	285^{o}K	196^{o}K
CIRA 1965 Temperatures	80 km	185^{o}K	185^{o}K	218^{o}K	218^{o}K	182^{o}K
	100 km	213^{o}K				

Table 6.1 Electron and neutral temperatures with relevant data.

to study the latitudinal variation of electron density. Rocket 14.246 was launched at noon, On June 17, 1965, as a part of a four rocket series, launched in April, June, September, and December, to study the seasonal changes in D- and E-region electron densities and electron collision frequencies. Details regarding these various rocket series and their results have been presented in Section 4.5.

The results of the application of Equations (6.9) and (6.10) to calculate T_e and T_n are given in Table 6.1. Comparison of electron and neutral temperatures listed in this table suggests that thermal equilibrium conditions exist in the D- and lower E-regions of the ionosphere. The probable error in the electron temperature computation depends on the zenith angle at the time of the rocket launch. Proper error compounding of the various measured parameters in Equation (6.9) revealed that for large zenith angles, $\chi \geq 85^{\circ}$, the probable error is about 23% whereas for small zenith angles, $\chi < 70^{\circ}$, the probable error is about 17%. At large zenith angles, a 10% error in the optical depth factor is introduced, which in turn affects the molecular oxygen concentration, and increases the probable error in T_e. The probable error in the computation of the neutral temperature by Equation (6.10) is the same as that involved in the extraction of the scale height from molecular oxygen densities. Systematic errors of absorption cross-section and zenith angle do not affect the scale height, but the non-ideal behavior of the ion chamber introduces a probable error of a few percent. Radiation other than Lyman-α in the bandpass of the ion chamber leads to an increase in the value of $n(O_2)$ at high altitudes, whereas

radiation that is absorbed less strongly than Lyman$_{\alpha}$ tends to decrease the value of $n(O_2)$ from its true value at lower altitudes (Smith and Weeks, 1965). Therefore the scale height of the molecular oxygen distribution possesses a probable error of a few percent. The same error may than be estimated for the neutral temperature.

For 14.145, 14.146, 14.231, and 14.246, the average neutral temperatures computed from the molecular oxygen scale heights are in good agreement with CIRA 1965 temperatures at the top of the mesopause. The probable error associated with the CIRA temperatures has been given by CIRA as $\pm 40^{\circ}K$ at 90 km.

However, 14.232, launched 14° south of 14.231, shows a large increase in temperature. Since both neutral and electron temperatures have been found in Equations (6.9) and (6.10) to be directly proportional to scale height, and since thermal equilibrium conditions are still met, the temperature variation may be explained in terms of the molecular oxygen scale height. The molecular oxygen measurements for 14.232 were made during the descent portion of the rocket trajectory since no data were collected during the ascent due to failure of the doors to eject on time. Furthermore, for this particular flight the sensitivity of the photometer was low and a 10% probable error may be attributed to the scale height value quoted in Table 6.1 (Weeks, private communication). If the ascent collision model is applied for the descent portion, re-calculation of the temperatures based upon the above yields an electron temperature of $255^{\circ}K$ compared to a neutral temperature of $257^{\circ}K$. This temperature is still higher than the neutral temperature quoted in

CIRA, but CIRA 1965 suggests a variation of $\pm 50^{\circ}K$ from the mean value of $213^{\circ}K$ at 100 km. In addition, by taking account of the latitude variation with a six-month change of date to apply CIRA 1965 values to the southern hemisphere, an additional $20^{\circ}K$ correction may be applied for the maximum variation at 60° latitude and 80 km altitude. This may then bring 14.232 results within reasonable limits.

7. SUMMARY OF OBSERVATIONS AND RESULTS

Below 100 km, the simplest method for the determination of electron temperature is derived from the consideration of the collision frequency of electrons with neutrals. This report has attempted to describe the experimental and analytical techniques involved in the measurement of the various parameters needed for the computation of electron and neutral temperatures. The results of the application of these methods have been given in Section 6.5.

In Table 6.1, though the measured electron collision frequency model for 14.232 is about 1.2 times larger than that for 14.231, this does not imply a difference in the neutral temperature. The measured electron collision frequency model for 14.231 agrees with that for 14.230, launched at a latitude of $29^{o}34'S$ in the same series. An identical procedure has been used for all rockets to extract the electron collision frequency model from the absorption data. Hence, the collision frequencies are proportional to the neutral densities, since the same factor relates the scale height of 14.232 to the other experiments.

Measurements made by Carver et al., (1964) from Woomera, Australia, (lat. $30^{o}S$, long. $136^{o}E$), show a scale height of 6.5 km which agrees with 14.231 measurements and northern hemisphere values. Moreover, measurements made by Kupperian et al., (1959) at Fort Churchill, Canada ($59^{o}N$) for a spring rocket experiment show a sudden change of scale height between 88 and 98 km, the same range as 14.232. In this range, a scale height of 8 km is obtained from the molecular oxygen concentration

measured at Fort Churchill. Above 98 km, the scale height decreases rapidly, and this has been interpreted as an indication of the dissociation level for molecular oxygen. The increase in temperature for 14.232 may then be a latitude effect combined with possible anomalous winter conditions. This latitude effect, as compared with Kupperian et al.'s results in the northern hemisphere, has been also observed by rocket grenade soundings at the lower altitudes (Nordberg et al., 1965).

The seasonal variation of temperature, again confirmed by grenade explosions, may be explained by the radiation unbalance theory proposed by Kellogg (1961). Heating of the region 70-100 km in winter at high latitudes may be due to a release of the energy of recombination of atomic oxygen which is carried downward by diffusion. This energy release mechanism has been verified by Young and Epstein (1962). Another noteworthy possible source of energy may be internal atmospheric gravity waves which, Hines (1965) suggests, might provide temperature increase near the 95 km level and explain the observed irregularities.

Furthermore, it may be possible to examine the effect of the increase of the temperature on the nitric oxide concentration, and therefore the electron density at the lower altitudes. Since an absolute measure of the electron density is available, a verification of the validity of the high temperature would be easily obtained. However, since the height range of the calculated temperatures for 14.232 is above 90 km, no effect on the nitric oxide concentration has been observed at this altitude.

It is obvious that more evidence should be accumulated to assert the increasing scale height below the dissociation level at high latitudes.

Finally, it should be noted that the rocket flights listed in Table 6.1 were launched under a wide variety of ionospheric conditions. The absorption recorded at one altitude differed from flight to flight. The collision frequency and hence the electron temperature, extracted from the absorption measurements, also varied from flight to flight. However, in all cases, thermal equilibrium conditions were found to exist in the D- and lower E-regions. This shows that thermal equilibrium exists at these altitudes regardless of the diurnal, seasonal, and latitudinal conditions of the lower ionosphere.

REFERENCES

Anderson, J.M.,and L. Goldstein (1956), Momentum transfer cross section and fractional energy loss in the collisions of slow electrons with nitrogen molecules, Phys. Rev. 102, 388-389.

Appleton, E.V. (1932), Wireless studies of the ionosphere, J. Instn. Elect. Engrs. 71, 642-650.

Belrose, J.S., and L.N. Hewitt (1964), Variation of collision frequency in the lowest ionosphere with solar activity, Nature, 267-269.

Bowhill, S.A. (1965a), Electron density measurements by the radio propagation technique, COSPAR Information Bulletin No. 17, ed. K. Maeda, 8-35.

Bowhill, S.A. (1965b), IQSY rocket studies of the C-, D-, and E-regions of the ionosphere, NASA-University Program Review Conference, Kansas City, Missouri, NASA SP-85.

Bowhill, S.A. (1966), A rocket experiment on the structure of Sporadic E, Radio Sci. 1, 187-190.

Bowhill, S.A., and E.R. Schmerling (1961), The distribution of electrons in the ionosphere, Advances in Electronics and Electron Phys. 15, 265-326.

Bowhill, S.A., and L.G. Smith (1965), Rocket observations of the lowest ionosphere at sunrise and sunset, presented at COSPAR, Buenos Aires.

Brace, L.H., N.W. Spencer, and A. Dalgarno (1965), Detailed behaviour of the mid-latitude ionosphere from the Explorer XVII satellite, Planet. Space Sci. 13, 647-666.

Bradbury, N.E., and R.A. Nielsen (1936), Absolute values of the electron mobility in hydrogen, Phys. Rev. 49, 388-393.

Budden, K.G. (1961), Radio Waves in the Ionosphere, University Press, Cambridge.

Burke, M.J., and E. Hara (1963), A table of C-script integrals for use with the generalized Appleton-Hartree magneto-ionic formulas, Defence Research Telecommunications Establishment, Ottawa, Canada, Report 1113.

Carver, J.H., P. Mitchell, E.L. Murray, and B.G. Hunt (1964), Molecular oxygen density and Lyman-α absorption in the upper atmosphere, J. Geophys. Res. 69, 3755-3756.

Chubb, T.A., E.T. Byram, H. Friedman, and J.E. Kupperian (1957), For ultraviolet radiation in the night sky, The Threshold of Space, ed. M. Zelikoff, Pergamon Press, London, 203-210.

CIRA 1965, COSPAR International Reference Atmosphere, 1965, North Holland Publishing Co., Amsterdam, 1965.

Colegrove, F.D., W.B. Hanson, and F.S. Johnson (1965), Eddy diffusion and oxygen transport in the lower thermosphere, J. Geophys. Res. 70, 4931-4941.

Crompton, R.W., and D.J. Sutton (1952), Experimental investigation of the diffusion of slow electrons in nitrogen and hydrogen, Proc. Roy. Soc. A215, 467-480.

Dalgarno, A., and J.W. Henry (1965), Electron temperatures in the D-region, Proc. of Roy. Soc. A288, 521-530.

Dalgarno, A., M.B. McElroy, and R.J. Moffett (1963), Electron temperature in the ionosphere, Planet. Space Sci. 11, 463-484.

Deeks, D.G. (1966), D-region electron distributions in middle latitudes deduced from the reflexion of long radio waves, Proc. Roy. Soc. A291, 413-437.

Dingle, R.B., D. Arndt, and S.K. Roy (1957), The integrals
$\mathcal{O}_p(x) = (p!)^{-1} \int_o^\infty \varepsilon^p(\varepsilon^2 + x^2)^{-1} e^{-\varepsilon} d\varepsilon$ and
$\mathcal{E}_p(x) = (p!)^{-1} \int_o^\infty \varepsilon^{-p}(\varepsilon^2 + x^2)^{-2} e^{-\varepsilon} d\varepsilon$ and their tabulation, Appl. Sci. Res. 6B, 155-164.

Eckhouse, R.H., Jr. (1964), A Fortran computer program for determining the earth's magnetic field, Electrical Engineering Research Lab. Engineering Experiment Station, University of Illinois, Urbana, Illinois.

Evans, J.V., and M. Lowenthal (1964), Ionospheric backscatter observations, Planet. Space Sci. 12, 915-944.

Fejer, J.A. (1962), The absorption of radio waves in the ionospheric D- and E-regions, Radio Wave Absorption in the Ionosphere, ed. N.C. Gerson, Pergammon Press, 260-274.

Friedman, H. (1960), Physics of the Upper Atmosphere, ed. J.A. Ratcliffe, 133-218 Academic Press, New York.

Gooch, J. (1965), Analog Faraday rotation data reduction system, Coordinated Science Laboratory Progress Report for June, July, and August 1965, 8-11.

Hall, L.A., K.R. Damon, and H.E. Hinterreger (1963), Solar extreme ultraviolet photon flux measurements in the upper atmosphere of August 1961, Space Research III, 745-759, North Holland Publishing Co., Amsterdam.

Hartree, D.R. (1931), The propagation of electro-magnetic waves in a refracting medium in a magnetic field, Proc. Cambridge Phil. Soc. 27, 143-162.

Healey, R.H., and J.W. Reed (1951), The Behavior of Slow Electrons in Gases, Amalgamated Wireless, Sydney

Hines, C.O. (1965), Dynamical heating of the upper atmosphere, J. Geophys. Res. 70, 177-183.

Huxley, L.G.H. (1959), A discussion of the motion in nitrogen of free electrons with small energies with reference to the ionosphere, J. Atmosph. Terrest. Phys. 16, 46-58.

Kane, J.A. (1959), Arctic measurements of electron collision frequencies in the D-region of the ionosphere, J. Geophys. Res. 64, 133-139.

Kellogg, W. (1961), Chemical heating above the polar mesopause in winter, J. Meteor. 18, 373-381.

Knoebel, H., D. Skaperdas, J. Gooch, B. Kirkwood, and H. Krone (1965), High resolution radio frequency measurements of Faraday rotation and differential absorption with rocket probes, ed. D. Skaperdas, Coordinated Science Laboratory, University of Illinois, Report R-273.

Kupperian, J.E., E.T. Byram, and H. Friedman (1959), Molecular oxygen densities in the mesosphere at Fort Churchill, J. Atmosph. and Terrest. Phys. 16, 174-178.

Nawrocki, P.J., K. Watanabe, and L.G. Smith (1961), The upper atmosphere, Geophysics Corp. of America, GCA Technical Report 61-13A.

Nicolet, M. (1959), Collision frequency of electrons in the terrestial atmosphere, Phys. of Fluids 2, 95-99.

Nielsen, R.A., and N.E. Bradbury (1937), Electron and negative low mobilities in oxygen, air nitrous oxides, and ammonia, Phys. Rev. 51, 69-75.

Nordberg, W., L. Katchen, J. Theon, and W.S. Smith (1965), Rocket observations of the structure of the mesosphere, J. Atmos. Sci. 22, 611-622.

Phelps, A.V., O.T. Fundingsland, and S.C. Brown (1951), Microwave determination of the probability of collision of slow electrons in gases, Phys. Rev. 84, 559-562.

Phelps, A.V., and J.L. Pack (1951), Electron collision frequencies in nitrogen and in the lower ionosphere, Phys. Rev. 3, 340-342.

Ratcliffe, J.A. (1959), The Magneto-ionic Theory and its Applications to the Ionosphere, University Press, Cambridge.

Rumi, G.C. (1962), Experiment Luxembourg: cross modulation at high latitude, low height, IRE Trans. Antennas Propag. 10, 594-607.

Salah, J.E., and S.A. Bowhill (1966), Electron densities and collision frequencies measured by rockets during the IQSY, Aeronomy Report No. 16, Aeronomy Laboratory, Dept. of Electrical Engineering, University of Illinois, Urbana, Illinois, (to be published).

Sears, R.D. (1963), Contribution of energetic photoelectrons in D-region non-equilibrium electron temperatures, J. Geophys. Res. 68, 5134-5142.

Seddon, J.C. (1958), Differential absorption in the D- and lower E-regions, J. Geophys. Res. 63, 209-216.

Sen, H.K., and A.A. Wyller (1960), On the generalization of the Appleton-Hartree magneto-ionic formulas, J. Geophys. Res. 65, 3931-3950.

Smith, L.G. (1965), Langmuir probes for measurements in the ionosphere, GCA Tech. Report No. 65-25N.

Smith, L.G. (1966), Rocket observations of Sporadic E and related features of the E-region, Radio Sci. 2, 178-186.

Smith, L.G., and L. Weeks (1965), Molecular oxygen densities from rocket measurements of Lyman-α absorption profiles, GCA Technical Report No. 65-10-N.

Smith, L.G., L.H. Weeks, and P.J. McKinnon (1965), Investigation of the D- and E-regions of the ionosphere during the IQSY, GCA Tech. Report No. 65-21-N.

Spencer, L.V., L.H. Brace, and G.R. Carignan (1962), Electron temperature evidence for non-thermal equilibrium in the ionosphere, J. Geophys. Res. 67, 157-175.

Swider, W., Jr. (1964), The determination of optical depth at large solar zenith distances, Planet. Space Sci. 12, 761-782.

Watanabe, K. (1958), UV absorption processes in upper atmosphere, Advances in Geophysics 5, ed. Landsberg, H.E., and J. Van Mieghem, Academic Press, 153-221.

Weeks, L. (1966), private communication.

Young, C., and E.S. Epstein (1962), Atomic oxygen in the polar winter mesosphere, J. Atmos. Sci. 19, 435-443.